Journal of Computational Science 92 (2025) 102733

Contents lists available at ScienceDirect

Journal of Computational Science

journal homepage: www.elsevier.com/locate/jocs

Optimal control applied to a dengue model incorporating symptomatic, asymptomatic, and severe cases with limited healthcare resources

Salamida Daudi [a], Eva Lusekelo [b], Mlyashimbi Helikumi [c], Steady Mushayabasa [d,e,*]

[a] Department of Mathematics, Humanities and Social Science, National Institute of Transport, Dar-es-Salaam, Tanzania
[b] Department of Mathematics, College of Natural and Mathematical Sciences, University of Dodoma, Dodoma, Tanzania
[c] Mbeya University of Science and Technology, Department of Mathematics and Statistics, College of Science and Technical Education, P.O. Box 131, Mbeya, Tanzania
[d] Department of Mathematics, School of Engineering and Technology, Harare Institute of Technology, P. O. Box BE 277, Ganges Road, Belvedere, Harare, Zimbabwe
[e] University of Zimbabwe, Department of Mathematics & Computational Sciences, P.O. Box MP 167 Mount Pleasant, Harare, Zimbabwe

ARTICLE INFO

MSC:
92B05
93A30
93C15

Keywords:
Dengue fever
Mathematical model
Limited medical resources
Optimal control theory

ABSTRACT

Dengue remains the most common arboviral disease globally, but the public health implications of different dengue clinical manifestations and the insufficiency of public health infrastructure are not well understood. Accounting for these factors provides valuable insights for the effective management of the disease. This study develops a novel mathematical model for dengue fever that incorporates various clinical manifestations, constraints imposed by limited medical resources, and preventive control strategies. We computed the basic reproduction number and examined its correlation with model parameters. Dynamical analysis revealed that the model exhibits a backward bifurcation. Using numerical techniques, we investigated the influence of varying control strategies, modeled as both time-dependent and non-time-dependent functions, on epidemic dynamics. In both scenarios, we identified threshold levels of intervention and the timelines required for disease extinction. These findings underscore the complexity of dengue dynamics and highlight the necessity of tailored intervention approaches for effective disease management.

1. Introduction

Dengue is widely regarded as the world's fastest-spreading vector-borne disease (VBD), responsible for over 390 million infections globally [1] and approximately 40,000 deaths annually [2]. The disease poses a significant public health challenge, particularly because of its rapid transmission dynamics and the expanding geographic range of its primary vectors, *Aedes aegypti* and *Aedes albopictus*. According to the World Health Organization (WHO), approximately half of the world's population is at risk of dengue infection, highlighting the widespread nature of this disease and its potential to affect both urban and rural communities [1–3]. Recent reports underscore the severity of the dengue situation in specific regions. For example, Brazil is currently experiencing the most severe dengue outbreak globally, with a reported 3,088,723 cases in 2023 alone [4]. Moreover, in the first two months of 2024, the country has already reported over one million cases, indicating an alarming escalation of the epidemic [4]. These figures underscore the urgent need for comprehensive, multidisciplinary research efforts to understand, prevent, and control dengue transmission effectively.

The clinical manifestations of dengue vary widely, ranging from mild constitutional symptoms to severe infections such as dengue hemorrhagic fever (DHF) and dengue shock syndrome (DSS) [5,6]. While asymptomatic infections are often mild and can be managed on an outpatient basis, DSS and DHF require hospitalization and specialized medical care in intensive care units [7]. The increasing frequency of dengue outbreaks, coupled with the inadequacy of public health infrastructure, has led to case fatality rates exceeding 1% in many regions [7,8]. Despite this, the public health implications stemming from the relationship between dengue clinical manifestations and infrastructure limitations remain poorly understood. A deeper understanding of these interactions is essential for developing effective intervention strategies.

* Corresponding author at: University of Zimbabwe, Department of Mathematics & Computational Sciences, P.O. Box MP 167 Mount Pleasant, Harare, Zimbabwe.
E-mail addresses: daudisalamida81@gmail.com (S. Daudi), lusekeloe@nm-aist.ac.tz (E. Lusekelo), mhelikumi@yahoo.co.uk (M. Helikumi), steadymushaya@gmail.com (S. Mushayabasa).

https://doi.org/10.1016/j.jocs.2025.102733
Received 15 April 2025; Received in revised form 15 July 2025; Accepted 14 October 2025
Available online 21 October 2025

Mathematical modeling has become an invaluable tool for studying the complex dynamics of dengue fever (DF). A comprehensive review of various models related to dengue transmission can be found in recent systematic reviews [9,10]. Broadly, these studies have investigated factors influencing dengue spread, including climate variability [11], human mobility [12], intervention strategies [13,14], and transmission routes [15,16]. Despite these advancements, there remains a notable gap in quantifying the impact of differing clinical manifestations and infrastructure limitations—especially given the high disease burden observed globally. To address this gap, in this work, we propose a novel mathematical model of dengue transmission and control that explicitly incorporates various clinical manifestations and the constraints imposed by limited public health infrastructure. Our approach builds upon the foundational work of Abdelrazec et al. [13], who analyzed the effects of limited medical resources on dengue dynamics but did not account for the heterogeneity of clinical presentations. Since not all dengue cases require hospitalization,it is crucial for the model to reflect these distinctions to accurately evaluate the role of resource limitations in disease progression and control.

Our modeling begins with a basic transmission framework that accounts for asymptomatic, symptomatic, and severe cases. We analyze the model's dynamical behavior by calculating the basic reproduction number and performing bifurcation analysis. Notably, our findings reveal that the model admits a backward bifurcation when the reproduction number is near one. This phenomenon indicates that simply reducing the reproduction number below unity may not be sufficient for disease eradication, highlighting the need for more aggressive and comprehensive control measures. This insight underscores the importance of understanding the underlying bifurcation dynamics when designing intervention strategies.

Motivated by this, we extend the initial model to incorporate the implementation of time-dependent preventive strategies and the effects of limited public health infrastructure. Current control measures for dengue include vector control interventions (such as larviciding and insecticide application), vaccination, and personal protective behaviors (like use of insect repellents and wearing long-sleeved clothing). However, given resource constraints in many endemic regions, we focus on strategies aimed at minimizing host-vector contact through resource-efficient, time-dependent control efforts. Since vector control can be costly and environmentally unfriendly, our model emphasizes host-focused interventions, which can be phased or scaled according to resource availability. These dynamic strategies offer greater adaptability to real-world limitations, enabling public health authorities to implement phased control efforts that are both effective and sustainable.

The structure of this paper is as follows: In the next section, we present the methods and analytical results, including the formulation of the basic mathematical model, the computation of the reproduction number, and the investigation of its stability properties. We then extend this framework to incorporate preventive control strategies and a nonlinear recovery rate function to reflect resource limitations. In Section 3, we conducted comprehensive simulation experiments using MATLAB to validate and support the analytical findings presented earlier. Finally, in Section 4, we summarize our main findings and discuss their implications for dengue control and future research directions.

2. Mathematical models

In this section, we introduce two mathematical models of dengue fever transmission. We begin with a basic model that captures the interactions between hosts (humans) and vectors (mosquitoes) under the assumption of constant intervention strategies. This foundational framework is subsequently extended to include constraints related to limited healthcare capacity and to account for time-dependent preventive measures, providing a more comprehensive representation of real-world dynamics.

2.1. The basic dengue transmission model

The dengue fever transmission model proposed in this study is governed by the following assumptions:

(A.1) Susceptible host acquire infection soley through being bitten by an infectious mosquito. Similarly, a susceptible mosquito becomes infected when it takes a blood meal from an infectious host [3].
(A.2) Once infected, a host incubates the disease for a certain period of time before they become infectious, after which they become infectious [9].
(A.3) Prior studies suggest that, upon completion of the incubation period, dengue patients present with different clinical manifestations. The common ones include asymptomatic cases (individuals infected but not showing noticeable symptoms), symptomatic cases (individuals displaying clinical signs such as fever, headache, muscle and joint pains, and rash), and severe cases (individuals experiencing complications such as plasma leakage, hemorrhage—known as dengue hemorrhagic fever—shock (dengue shock syndrome), and even organ failure) [17]. Therefore, the proposed model accounts for these clinical variations.
(A.4) While most dengue cases can be treated at home with pain medication, individuals with severe dengue often require hospitalization [6]. Therefore, the proposed model incorporates a compartment for hospitalized patients.
(A.5) In 2023, Brazil registered a total of 1,658,814 suspected cases of dengue, with 1094 deaths. Most of these deaths occurred among severely infected patients [18]. Therefore, in the proposed model, we assume that both undetected and detected severe patients are at risk of disease-related death.
(A.6) It is well known that once mosquitoes are infected with the disease, they remain infectious for their entire lifespan, and they do not suffer disease-related death.

Based on the above assumptions, we consider a framework that subdivides the total human population at time t, $N_h(t)$, into seven compartments: susceptible individuals S_h; exposed individuals $E_h(t)$; asymptomatic infectious individuals $I_{h1}(t)$; clinically infected individuals with mild symptoms $I_{h2}(t)$; severely infected individuals $I_{h3}(t)$; hospitalized individuals $Q_h(t)$; and recovered individuals $R_h(t)$. The vector population is subdivided into three compartments: susceptible mosquitoes $S_v(t)$, exposed mosquitoes $E_v(t)$, and infectious mosquitoes $I_v(t)$. Consequently, we propose the following system of ordinary differential equations (ODEs):

$$\frac{dS_h(t)}{dt} = \Lambda_h - \frac{\beta_{vh} I_v}{N_h} S_h - \mu_h S_h, \tag{2.1}$$

$$\frac{dE_h(t)}{dt} = \frac{\beta_{vh} I_v}{N_h} S_h - (\mu_h + \gamma_h) E_h, \tag{2.2}$$

$$\frac{dI_{h1}(t)}{dt} = p_1 \gamma_h E_h - (\mu_h + \sigma_{h1}) I_{h1}, \tag{2.3}$$

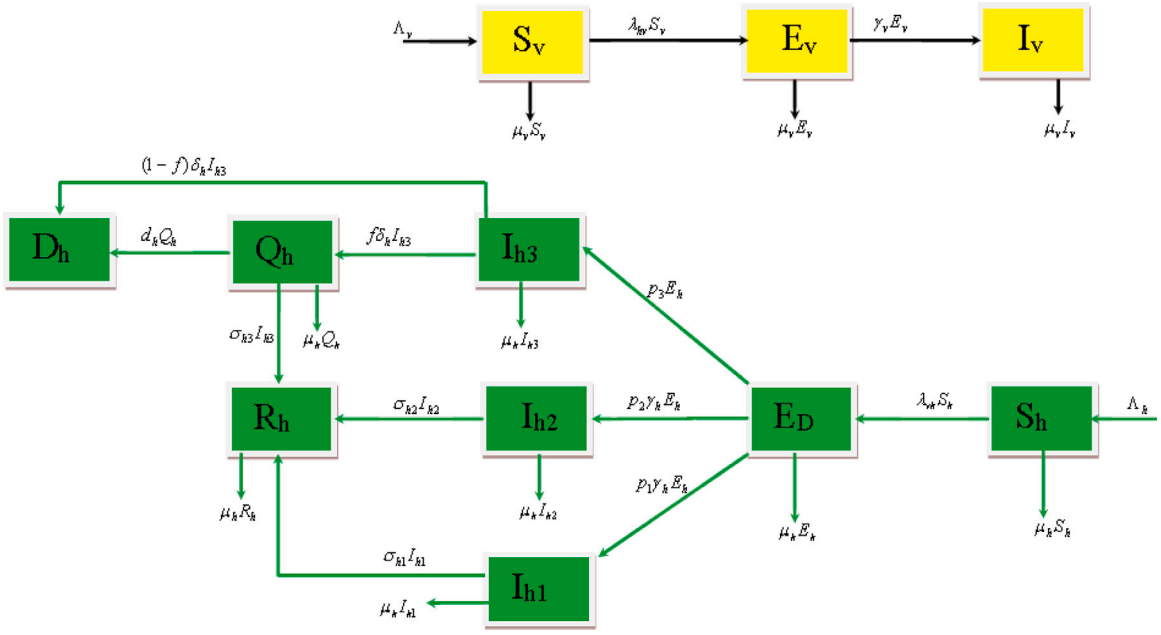

Fig. 1. Model flow diagram showing the interaction of the host and vector populations, with $\lambda_{vh} = \frac{\beta_{vh} I_v}{N_h}$ and $\lambda_{hv} = \frac{\beta_{hv}(I_{h1} + I_{h2} + I_{h3} + Q_h)}{N_h}$. The compartment $D_h(t)$ represents deaths.

$$\frac{dI_{h2}(t)}{dt} = p_2\gamma_h E_h - (\mu_h + \sigma_{h2})I_{h2}, \tag{2.4}$$

$$\frac{dI_{h3}(t)}{dt} = p_3\gamma_h E_h - (\mu_h + \alpha_h + \delta_h)I_{h3}, \tag{2.5}$$

$$\frac{dQ_h(t)}{dt} = \alpha_h I_{h3} - (\mu_h + \sigma_{h3} + d_h)Q_h, \tag{2.6}$$

$$\frac{dR_h(t)}{dt} = \sigma_{h1} I_{h1} + \sigma_{h2} I_{h2} + f\delta_h I_{h3} + \sigma_{h3} Q_h - \mu_h R_h, \tag{2.7}$$

$$\frac{dS_v(t)}{dt} = \Lambda_v - \frac{\beta_{hv}(I_{h1} + I_{h2} + I_{h3} + Q_h)}{N_h} S_v - \mu_v S_v, \tag{2.8}$$

$$\frac{dE_v(t)}{dt} = \frac{\beta_{hv}(I_{h1} + I_{h2} + I_{h3} + Q_h)}{N_h} S_v - (\mu_v + \gamma_v)E_v, \tag{2.9}$$

$$\frac{dI_v(t)}{dt} = \gamma_v E_v - \mu_v I_v, \tag{2.10}$$

with initial conditions:

$$\begin{aligned} S_h(0) &= S_{h0} \geq 0, \quad E_h(0) = E_{h0} \geq 0, \quad I_{h1}(0) = I_{h10} \geq 0, \quad I_{h2}(0) = I_{h20} \geq 0, \quad I_{h3}(0) = I_{h30} \geq 0, \\ Q_h(0) &= Q_{h0} \geq 0, \quad R_h(0) = R_{h0} \geq 0, \quad S_v(0) = S_{v0} \geq 0, \quad E_v(0) = E_{v0} \geq 0, \quad I_v(0) = I_{v0} \geq 0. \end{aligned}$$

In model (2.1)–(2.10), the subscripts h and v denote variables or parameters associated with the host and vector, respectively. The parameter Λ_i represents the inflow into the susceptible population; μ_i is the natural mortality rate; and γ_i is the incubation rate. The parameter β_{ij} denotes the disease transmission rate for $i \neq j$, where $i, j \in \{h, v\}$. Parameters p_1, p_2, and p_3 denote the proportions of asymptomatic, symptomatic, and severe cases, respectively. The parameters σ_{h1} and σ_{h2} represent the recovery rates of asymptomatic and symptomatic patients, respectively. Undetected severely infected individuals are assumed to have an average infectious period of $1/\delta_h$ units of time, and their probability of survival is modeled by f. If $f = 0$, it implies that severely infected individuals have zero chance of survival. Furthermore, severely infected patients are detected and hospitalized at rate α, and they recover at rate σ_{h3}. Based on these assumptions the proposed model takes the form (Fig. 1 depicts the model flow diagram):

One can easily verify that the domain of biological interest is of model (2.1)–(2.10) is:

$$\Omega = \left\{ \begin{pmatrix} (S_h(t),\ E_h(t)\ I_{h1}(t)\ I_{h2}(t)\ I_{h3}(t)\ Q_h(t),\ R_h(t)) \in N_h(t), \\ (S_v(t),\ E_v(t),\ I_v(t)) \in N_v(t) \end{pmatrix} \in \mathbb{R}_+^{10} \middle| \begin{array}{l} 0 \leq N_h(t) \leq \dfrac{\Lambda_h}{\mu_h}, \\ 0 \leq N_v(t) \leq \dfrac{\Lambda_v}{\mu_v}. \end{array} \right\} \tag{2.11}$$

Thus, system (2.1)–(2.10) with non-negative initial conditions has a unique solution that is non-negative and bounded from above for all ≥ 0.

2.1.1. The reproduction number

The reproduction number remains a fundamental threshold parameter in epidemiological models. In this study, we employed the next-generation matrix method [19] (see Appendix A) to derive the basic reproduction number of system (2.1)–(2.10), resulting in the following expression:

$$\mathcal{R}_0 = \sqrt{\frac{\beta_{hv}\Lambda_v\mu_h}{\Lambda_h\mu_v}\frac{\gamma_h}{m_1}\left(\frac{p_1}{m_2} + \frac{p_2}{m_3} + \frac{p_3}{m_4} + \frac{p_3\alpha_h}{m_4 m_5}\right)\frac{\beta_{vh}\gamma_v}{\mu_v m_6}}, \tag{2.12}$$

Table 1
Interpretation of model parameters and their baseline values adopted from literature.

Symbol	Biological definition	Unit	Baseline value	Source
Λ_h	Human recruitment rate	day^{-1}	869 – 1105	[14]
Λ_v	Mosquito recruitment rate	day^{-1}	400 – 5000	[24]
μ_h	Natural mortality rate of humans	$year^{-1}$	$[\frac{1}{50}, \frac{1}{70}]$	[9]
μ_v	Natural mortality rate of mosquitoes	day^{-1}	0.02 – 0.009	[15]
γ_h	Latent period of humans	day^{-1}	0.125 – 0.25	[15]
γ_v	Latent period of mosquitoes	day^{-1}	0.1(0 – 1)	[15]
α_h	Rate of hospitalization	day^{-1}	0.01 – 0.02	[14]
d_h/δ_h	Disease-related death rate	day^{-1}	0.005(0 – 1)	[11]
σ_{h1}	Recovery rate of asymptomatic patients	day^{-1}	1/5(0 – 1)	[15]
σ_{h2}	Recovery rate of mild infected patients	day^{-1}	1/6(0 – 1)	[15]
σ_{h3}	Recovery rate of hospitalized patients	day^{-1}	1/10(0 – 1)	[15]
p_1	Fraction of asymptomatic cases	–	0.85(0 – 1)	[6]
p_2	Fraction of symptomatic cases	–	0.1(0 – 0.5)	[6]
p_3	Fraction of severe cases	–	0.05(0.001 – 0.005)	[6]
β_{vh}	Mosquito-to-Human infection rate	day^{-1}	0.2(0.01 – 0.5)	[13]
β_{hv}	Human-to-mosquito infection rate	day^{-1}	0.1(0.01 – 0.75)	[13]
α_h	Hospitalization rate	day^{-1}	0.01(0 – 1)	[13]
f	Survival probability of severely infected patients	–	0.0001(0 – 1)	Assumed

where

$$m_1 = (\gamma_h + \mu_h), \quad m_2 = (\mu_h + \sigma_{h1}), \quad m_3 = (\mu_h + \sigma_{h2}),$$
$$m_4 = (\mu_h + \alpha_h + \delta_h), \quad m_5 = (\mu_h + \sigma_{h3} + d_h), \quad m_6 = (\mu_v + \gamma_v).$$

The interpretation of terms in $\mathcal{R}_0$ is as: $\frac{1}{\mu_v}$ is the average life span of mosquitoes, $\frac{\gamma_v}{\mu_v+\gamma_v}$ is the probability of exposed vector to survive that state and become infections, $\frac{\gamma_h}{\mu_h+\gamma_h}$ is the probability of exposed human to survive that state and become infections, $\frac{\Lambda_v\mu_h}{\Lambda_h\mu_v}$ is the ratio of vectors to hosts, $\frac{p_1}{\mu_h+\sigma_{h1}}$ is the average infectious duration of asymptomatic infectious patients, $\frac{p_2}{\mu_h+\sigma_{h2}}$ is the average infectious period of a fraction p_2 of mildly infected individuals, $\frac{p_3}{\mu_h+\alpha_h}$ is the average infectious period of a fraction p_3 of undetected severely infected individuals, $\frac{\alpha_h}{(\mu_h+\alpha_h)}$ is the probability that a severely infected individual is detected and hospitalized, the average infectious period on hospitalized individuals is $\frac{1}{\mu_h+\sigma_{h3}+d_h}$ is the average infectious period of a fraction p_3 of severely infected patients, β_{vh} and β_{hv} denote the transmission rates of infection from humans to vectors and from vectors to humans, respectively.

2.1.2. Parameter values and initial population levels

Due to the unavailability and scarcity of data, we adopted parameter values and initial population levels from published peer-reviewed articles or from dengue expert suggestions [6,11,14,15,20]. Most importantly, we made use of a recent 10-year systematic scoping review of mathematical models for dengue fever epidemiology [9]. This review provides a detailed discussion on dengue fever parameters and their ranges. To enhance the model's robustness, we subjected these parameters to sensitivity analysis. In particular, we set the following initial conditions: $S_{h0} = 1000$, $E_{h0} = 500$, $I_{h1} = 50$, $I_{h2} = 20$, $I_{h3} = 20$, $Q_{h0} = 0$, $R_{h0} = 0$, $D_{h0} = 0$, $S_{v0} = 10,000$, $E_{v0} = 500$, and $I_{v0} = 100$. Parameter values are provided in Table 1. The following is a discussion of some of the model parameters:

- $p_k,\ k = 1, 2, 3$: The majority of prior studies suggest that approximately 50% to 85% of dengue infections are asymptomatic, 20% to 50% are symptomatic, and severe cases typically constitute about 1% to 5% of all dengue infections [6]. However, it is worth noting that these proportions can vary depending on factors such as age, immune status, dengue serotype, and prior exposure.
- $1/\gamma_v$: The time required for a mosquito exposed to the virus to become infectious, known as the extrinsic incubation period (EIP), has been investigated through various extensive experiments. It is generally referenced as being 8–12 days [20]. In this study, we set this parameter to 10 days.
- $1/\gamma_h$: Similar to the EIP, the time between human infection and the onset of symptoms—also known as the intrinsic incubation period (IIP)—has been extensively investigated experimentally. It is generally believed to be in the range of 4–10 days [20]. In this study, we set this parameter to 8 days.
- $\sigma_{hk},\ k = 1, 2, 3$: The average infectious period of asymptomatic and symptomatic patients is generally in the range of 3–12 days [9]. However, there is a paucity of data on the mean hospital stay for severely infected individuals. In one study, the mean hospital stay ($1/\sigma_{h3}$) was estimated to be 4.88 ± 2.74 days [5]. In this study, we set $1/\sigma_{h3} = 10$ days, with the upper and lower bounds as 0 and 1, as presented in [9]. We also set the mean recovery times for asymptomatic and symptomatic patients as 5 and 6 days, respectively.
- $1/\mu_v$: Prior studies estimate the lifespan of adult mosquitoes to be in the range of 7.7–30 days [9,21–23]. In this study, we set this value to 10 days.
- β_{ij} for $i \neq j$, where $i, j \in \{h, v\}$: The disease transmission rate in vector-borne diseases is a product of the vector biting rate and the probability of infection transmission following contact. In prior studies, this parameter is generally believed to be in the range of 0–0.75 per day for host-to-vector transmission and 0–0.5 per day for vector-to-host transmission [9].

2.1.3. Bifurcation analysis

Based on Theorem 2 in [19], one can easily verify that the disease-free equilibrium (DFE) is locally asymptotically stable when $\mathcal{R}_0 < 1$. However, to establish the global stability of the DFE, a bifurcation analysis is necessary. Carrying out such an analysis is motivated by outcomes from prior studies, which suggest that a vector-borne disease model coupling standard incidence with disease-related mortality of the host can exhibit a backward bifurcation [13]. In simple terms, a backward bifurcation is a scenario where a stable endemic equilibrium co-exists with a disease-free

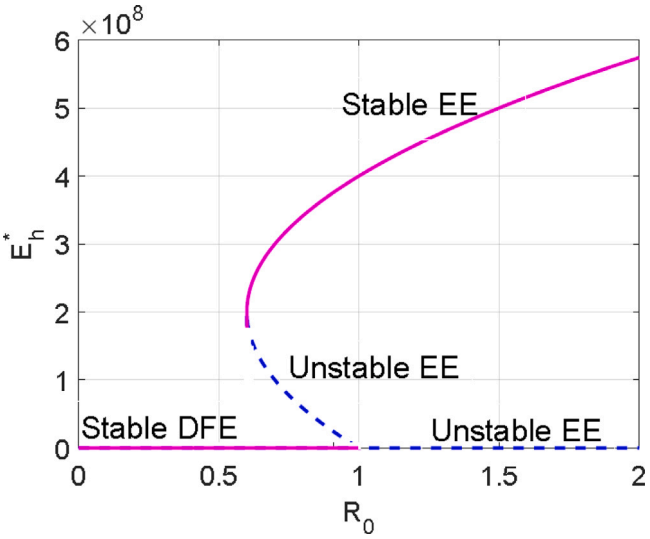

Fig. 2. Bifurcation diagram of model (2.1)–(2.10) showing the existence of a backward bifurcation at $\mathcal{R}_0 = 1$. DFE and EE represents the disease-free equilibrium point and the endemic equilibrium point, respectively. We set $\beta_{hv} = 2 \times 10^{-3}$, and $\beta_{hv} = 1.5 \times 10^{-3}$ and all other parameter values are as in Table 1.

equilibrium [13]. Based on extensive calculations presented in Appendix B, we conclude that the proposed model indeed admits a backward bifurcation, as indicated in prior studies [13,25]. We illustrate this phenomenon by simulating model (2.1)–(2.10) using a set of parameter values listed in Table 1, with the results depicted in Fig. 2.

Biologically speaking, the simulation results in Fig. 2 imply that reducing $\mathcal{R}_0$ below unity, although necessary, is not sufficient to ensure disease eradication. Therefore, additional intervention efforts are required to effectively manage dengue transmission, such as the implementation of time-dependent control strategies. Overall, recognizing the potential for backward bifurcation is critical for public health planning, as it underscores the importance of implementing sufficiently strong interventions beyond merely reducing the reproductive number to ensure successful disease eradication.

2.2. The optimal control problem

2.2.1. Problem formulation

Current control strategies for dengue transmission encompass a variety of measures aimed at reducing disease spread. These include: (i) vector control interventions, such as the elimination of breeding sites, larviciding, and the application of insecticides (e.g., fogging or space spraying) to decrease adult mosquito populations—particularly during outbreaks; (ii) personal protective measures, which involve the use of insect repellents containing active ingredients like picaridin, wearing long-sleeved clothing and long pants to minimize skin exposure, and installing window and door screens to prevent mosquito entry [23]; and (iii) vaccination, with Dengvaxia (CYD-TDV) currently being the only licensed dengue vaccine. Dengvaxia is recommended for individuals aged 9–45 years who have confirmed prior dengue infection in certain countries [26].

Despite the historical success of these interventions, vector control measures are often more expensive and pose environmental concerns compared to personal protection and vaccination. The extensive use of insecticides, in particular, has been associated with the emergence of insecticide-resistant mosquito populations [27], which can undermine control efforts and lead to increased costs and ecological impacts. Given the limited budgets typically available for dengue control, it is crucial to evaluate how personal protection and vaccination strategies can influence dengue transmission dynamics and optimize resource allocation. To this end, in this section, we formulate an optimal control problem based on the existing model Eqs. (2.1)–(2.10). We introduce a control variable $u(t)$, representing the combined effect of personal protection and vaccination efforts, which varies over time. This control reduces the forces of infection in both the vector and human populations by a factor of $(1 - u(t))$. Specifically, the transmission rates are modulated by this control function, enabling the assessment of different intervention intensities and their impacts on disease dynamics within a cost-effective framework.

Additionally, we modified the model Eqs. (2.1)–(2.10) to incorporate the limitations imposed by constrained medical healthcare resources. Specifically, we redefined the hospitalization rate α_h, which was previously considered a constant, as a nonlinear function that captures the saturation effect due to finite healthcare capacity. The modified form is given by:

$$\alpha_h(K_h, I_{h3}) = \alpha_{h0} + (\alpha_{h1} - \alpha_{h0})\frac{K_h}{K_h + I_{h3}}, \tag{2.13}$$

where α_{h0} and α_{h1} denote the minimum and maximum hospitalization rates, respectively. The parameter K_h represents the maximum capacity of the healthcare system, such as the total number of available hospital beds or medical resources capable of accommodating severe cases.

This functional form exhibits several important properties, which are critical for understanding the model dynamics:

- **Monotonicity with respect to I_{h3}**: The derivative of $\alpha_h(K_h, I_{h3})$ with respect to I_{h3} is given by:

$$\frac{\partial \alpha_h(K_h, I_{h3})}{\partial I_{h3}} = -(\alpha_{h1} - \alpha_{h0})\frac{K_h}{(K_h + I_{h3})^2} < 0, \tag{2.14}$$

  which indicates that α_h is a decreasing function of I_{h3}. Practically, this implies that as the number of severe cases I_{h3} increases, the rate at which these individuals can be hospitalized diminishes. This reflects real-world limitations where healthcare systems become overwhelmed, leading to a reduced capacity to admit new severe patients due to resource constraints.

Table 2
Interpretation of additional model parameters and their baseline values adopted from literature.

Symbol	Biological definition	Unit	Baseline value	Source
K_h	Hospitalbed population ratio		$0-20$	[13]
α_{h0}	Minimum hospitalization rate	day^{-1}	$0.01(0,1)$	[13]
α_{h1}	Maximum hospitalization rate	day^{-1}	$0.4(\alpha_{h0},10)$	[13]

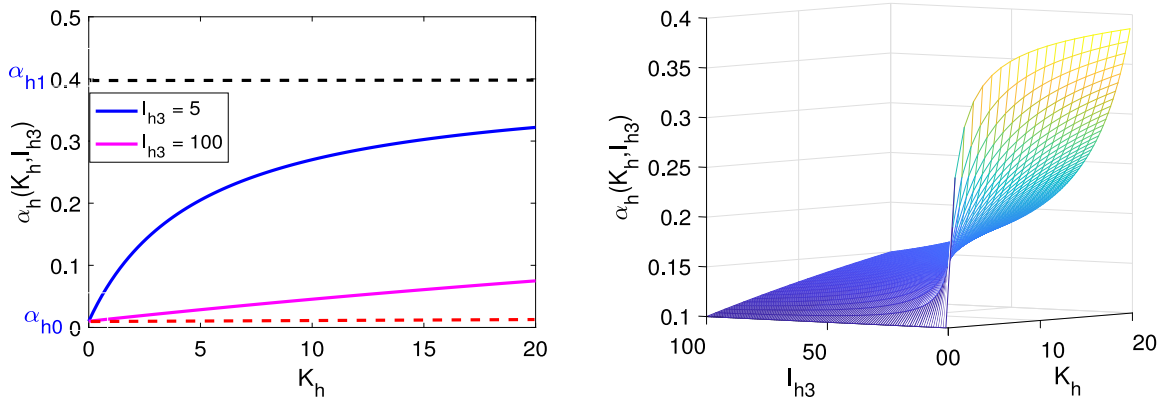

Fig. 3. The curve of hospitalization rate $\alpha_h(K_h, I_{h3})$ obtained using parameter values in Table 2.

- **Dependence on healthcare capacity** K_h: The partial derivative of α_h with respect to K_h is:

$$\frac{\partial \alpha_h(K_h, I_{h3})}{\partial K_h} = (\alpha_{h1} - \alpha_{h0}) \frac{I_{h3}}{(K_h + I_{h3})^2} > 0, \tag{2.15}$$

  which demonstrates that increasing the healthcare capacity K_h enhances the hospitalization rate, reflecting improved access to hospital care as resources expand.
- **Saturation behavior and boundedness and** : The function $\alpha_h(K_h, I_{h3})$ approaches a saturation limit as I_{h3} becomes large relative to K_h. Specifically,

$$\lim_{I_{h3}\to\infty} \alpha_h(K_h, I_{h3}) = \alpha_{h0}, \qquad \text{and} \qquad \lim_{I_{h3}\to 0} \alpha_h(K_h, I_{h3}) = \alpha_{h1}, \tag{2.16}$$

  which indicates that beyond a certain point, increasing the number of severe cases does not proportionally increase the hospitalization rate due to capacity limits. Conversely, when I_{h3} is small relative to K_h, the hospitalization rate approaches its maximum α_{h1}.

In a nutshell, this nonlinear formulation of α_h encapsulates the realistic constraints imposed by finite healthcare resources, illustrating how capacity limitations impact hospitalization rates as the severity of the epidemic evolves. Parameter values adopted from the literature (see Table 2) are used to graphically demonstrate the relationship between $\alpha_h(K_h, I_{h3})$ and I_{h3}, providing insights into the critical interplay between disease severity and healthcare capacity. The output is in Fig. 3. From the illustration we can observe that if I_{h3} is less than the hospital's carrying capacity, then the hospitalization rate increases and approaches its maximum value, denoted by α_{h1}. Conversely, when I_{h3} exceeds the hospital's carrying capacity, the hospitalization rate decreases and converges toward its minimum value, α_{h0}. Overall, this indicates that the hospitalization rate function $\alpha_h(K_h, I_{h3})$ is bounded above and below, with these bounds determined by the capacity constraints and the values of I_{h3}. This behavior reflects the intuitive understanding that hospital resources impose natural limits on hospitalization rates, which adjust dynamically depending on the current number of infected individuals relative to hospital capacity.

2.2.2. *The objective functional*

In developing response plans to mitigate the spread of dengue fever, policymakers aim to minimize the number of infectious hosts over a finite time interval $[0, t_f]$, while also minimizing the implementation costs. Therefore, a mathematical objective function is proposed as follows:

$$J(u) = \int_0^{t_f} \left(I_{h1}(t) + I_{h2}(t) + I_{h3}(t) + Q_h(t) + \frac{A}{2} u(t)^2 \right) dt, \tag{2.17}$$

subject to the constraints:

$$\frac{dS_h(t)}{dt} = \Lambda_h - (1-u(t)) \frac{\beta_{vh} I_v}{N_h} S_h - \mu_h S_h, \tag{2.18}$$

$$\frac{dE_h(t)}{dt} = (1-u(t)) \frac{\beta_{vh} I_v}{N_h} S_h - (\mu_h + \gamma_h) E_h, \tag{2.19}$$

$$\frac{dI_{h1}(t)}{dt} = p_1 \gamma_h E_h - (\mu_h + \sigma_{h1}) I_{h1}, \tag{2.20}$$

$$\frac{dI_{h2}(t)}{dt} = p_2 \gamma_h E_h - (\mu_h + \sigma_{h2}) I_{h2}, \tag{2.21}$$

$$\frac{dI_{h3}(t)}{dt} = p_3 \gamma_h E_h - (\mu_h + \delta_h) I_{h3} - \alpha_h(K_h, I_{h3}) I_{h3}, \tag{2.22}$$

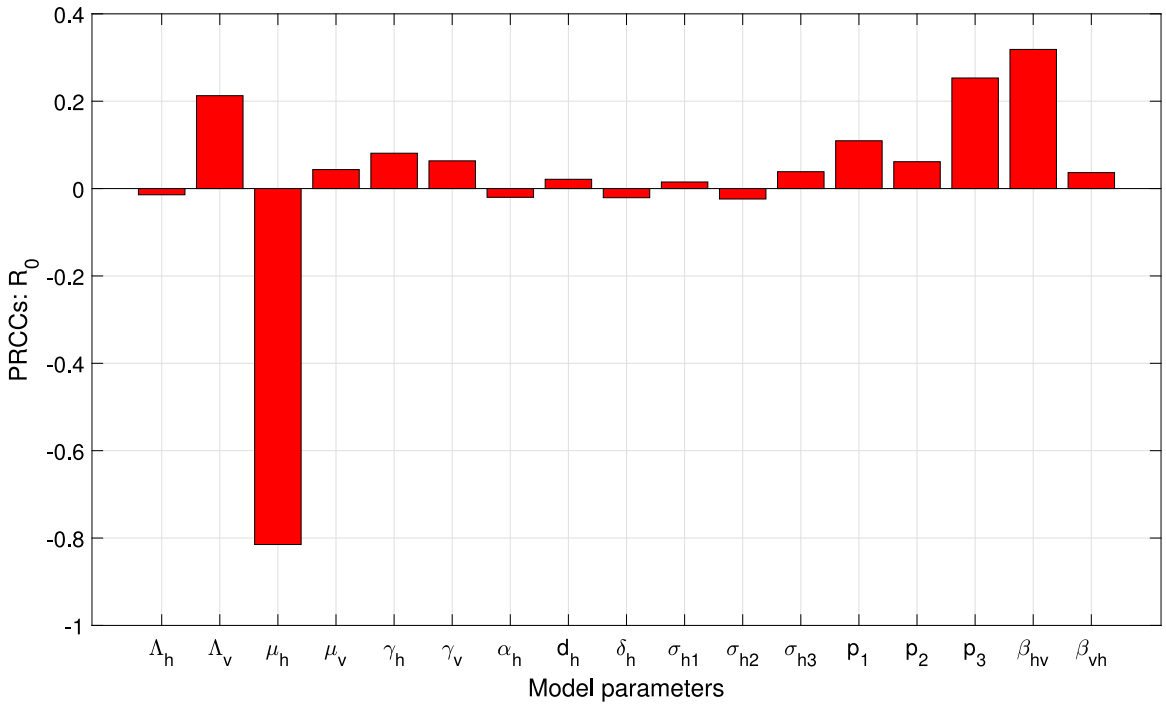

Fig. 4. Global sensitivity analysis of the reproduction number ($\mathcal{R}_0$).

$$\frac{dQ_h(t)}{dt} = \alpha_h(K_h, I_{h3})I_{h3} - (\mu_h + \sigma_{h3} + d_h)Q_h, \tag{2.23}$$

$$\frac{dR_h(t)}{dt} = \sigma_{h1}I_{h1} + \sigma_{h2}I_{h2} + f\delta_h I_{h3} + \sigma_{h3}Q_h - \mu_h R_h, \tag{2.24}$$

$$\frac{dS_v(t)}{dt} = \Lambda_v - (1-u(t))\frac{\beta_{hv}(I_{h1}+I_{h2}+I_{h3}+Q_h)}{N_h}S_v - \mu_v S_v, \tag{2.25}$$

$$\frac{dE_v(t)}{dt} = (1-u(t))\frac{\beta_{hv}(I_{h1}+I_{h2}+I_{h3}+Q_h)}{N_h}S_v - (\mu_v+\gamma_v)E_v, \tag{2.26}$$

$$\frac{dI_v(t)}{dt} = \gamma_v E_v - \mu_v I_v. \tag{2.27}$$

Here our goal in applying optimal control theory to model (2.18)–(2.27) is to minimize the number of new infection in the host population at minimal costs. The control functions $u(t)$ is defined over the interval $[0, t_f]$, where $0 \le u(t) \le 1$ and t_f represents the end time of the control. Parameter A, denotes the nonnegative weight constant. Thus, A represent relative cost of interventions to apply each control campaign over $[0, t_f]$. Our optimal control problem seeks to determine an optimal control solution capable of minimizing the population of severely infected individuals at minimal implementation costs.

Let u^* be the optimal control pair. Thus, we aim to identify a set of control functions such that $J(u^*) = \min J(u), \quad (u) \in \mathcal{W}$, subject to system (2.18)–(2.27), where $\mathcal{W}$ is the set of measurable functions defined from $[0, t_f]$ to $[0, 1]$. By using Pontryagin's Maximum Principle [28], we have the Hamiltonian function

$$\mathcal{H} = I_{h1} + I_{h2} + I_{h3} + Q_h + \frac{A}{2}u^2 + \sum^{10} \lambda_i g_i, \tag{2.28}$$

where λ_j, $j = 1, 2, \ldots, 10$ are the adjoint variables satisfying the adjoint system (2.18)–(2.27), and g_j denotes the right-hand sides of system (2.18)–(2.27), which corresponds to the ith state variable equation. Thus, given an optimal control solution (u^*), there exists adjoint functions, $\lambda_i(t)$, for $i = 1, 2, \ldots, 10$ corresponding to the states S_h, E_h, I_{h1}, I_{h2}, I_{h3}, Q_h, R_h, S_v, E_v, and I_v respectively. In Appendix C, we obtain the necessary conditions for optimality.

3. Numerical results

3.1. Sensitivity analysis of the reproduction number

In this subsection, we investigate the relationship between model parameters and $\mathcal{R}_0$, in order to identify model parameters that significantly influence disease transmission potential. Latin hypercube sampling (LHS) technique and partial rank correlation (PRCC) method are used in the analysis. To compute the PRCC, we used the Matlab implementation of the PRCC function developed in [29]. The function was run on the 1000 samples from Table 1 and the output is presented in Fig. 4. From the results we can note that $\mathcal{R}_0$ is positively correlated to majority of the model parameters that define it, however, of these parameters, mosquito recruitment rate (Λ_v), disease transmission rate of humans to vectors and the proportion of severely infected individuals (p_3). Increasing these parameters significantly increases $\mathcal{R}_0$. In contrast, we can note that an increase in natural mortality of the host significantly decreases $\mathcal{R}_0$. In Fig. 5, we used the LHS to further highlight the correlation between $\mathcal{R}_0$ and the individuals parameters which were identified in Fig. 4.

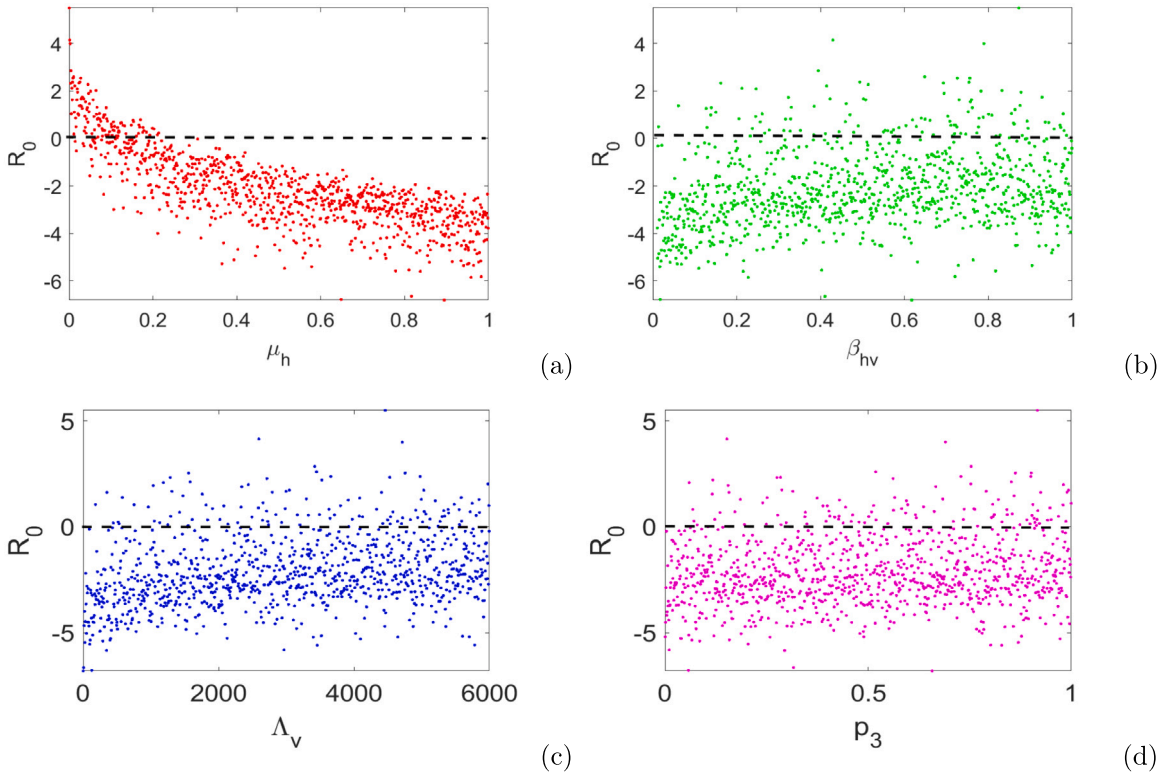

Fig. 5. Latin hypercube sampling output showing the relationship between $\mathcal{R}_0$ and individuals parameters.

3.2. Effects of severe cases on epidemic dynamics

Holding all other model parameters constant, we examined the variability in the epidemic dynamics due to changes in the proportion of infectious individuals by simulating model (2.1)–(2.10) using parameter values from Table 1. In particular, we focused on variations in the fraction of severely infected individuals (Fig. 6). The results show that an increase in p_3, representing the proportion of severely infected individuals, leads to an increase in the population of infectious individuals. Notably, for exposed, asymptomatic, and mild infectious patients, changes in parameters p_k (where $k = 1, 2, 3$) do not alter the peak period of cases, which occurs around 180 days. However, variations in p_k are associated with a delay in the peak period for severe and hospitalized patients, resulting in a delay of approximately 20 days.

Most importantly, our findings indicate that when an outbreak occurs in a community comprising a higher population of individuals with underlying health conditions, the impacts of the disease are significantly more severe. For instance, if $p = 0.05$ (5%), the number of death cases increases from zero to just below 400,000 over a duration of 300 days. Furthermore, increasing p_3 by an additional 5% doubles the number of death cases, highlighting the critical importance of underlying health conditions in the severity of dengue outbreaks.

3.3. Effects of variability in treatment rate when medical resources are unlimited on disease dynamics

Next, we simulated model (2.1)–(2.10) using parameter values from Table 1 to examine the implications of variability in epidemic dynamics under an unlimited treatment rate, which is represented by the parameter α_h. The results of this simulation are presented in Fig. 7. The findings indicate that increasing the treatment rate, under conditions of unlimited medical resources, significantly reduces both the infected population and the number of deaths over time. For instance, if $\alpha_h = 0.2$, approximately 50,000 deaths are projected over a duration of 300 days. Additionally, we observed that the peak period of the infectious population occurs between 150 and 200 days. This illustrates the critical role that effective treatment rates play in managing epidemic dynamics, emphasizing that enhanced medical interventions can substantially mitigate the impact of the disease on public health outcomes.

3.4. Simulation results for the optimal control problem

In this subsection, we examined the effect of combining time-dependent preventative strategies with the hospitalization of severely infected patients under limited medical resources. The numerical solutions were obtained after solving the optimality system (2.18)–(2.27) from the state and costate equations. The technique used is commonly known as the forward–backward sweep iterative method [30]. The first step of the forward–backward sweep method entails solving of the state equations with a guess for the controls over the simulated time using fourth-order Runge–Kutta scheme. "The controls are then updated by using a convex combination of the previous controls and the value from the characterizations of the controls. This process is repeated and iterations are ceased if the values of the unknowns at the previous iterations are very close to the ones at the present iterations" [30]. Table 3, presents the essential steps carried out, for a detailed discussion we refer the reader to [30]. We simulated the model (2.18) while changing the cost of implementing preventive strategies, denoted as A. The results are shown in Figs. 8 and 9.

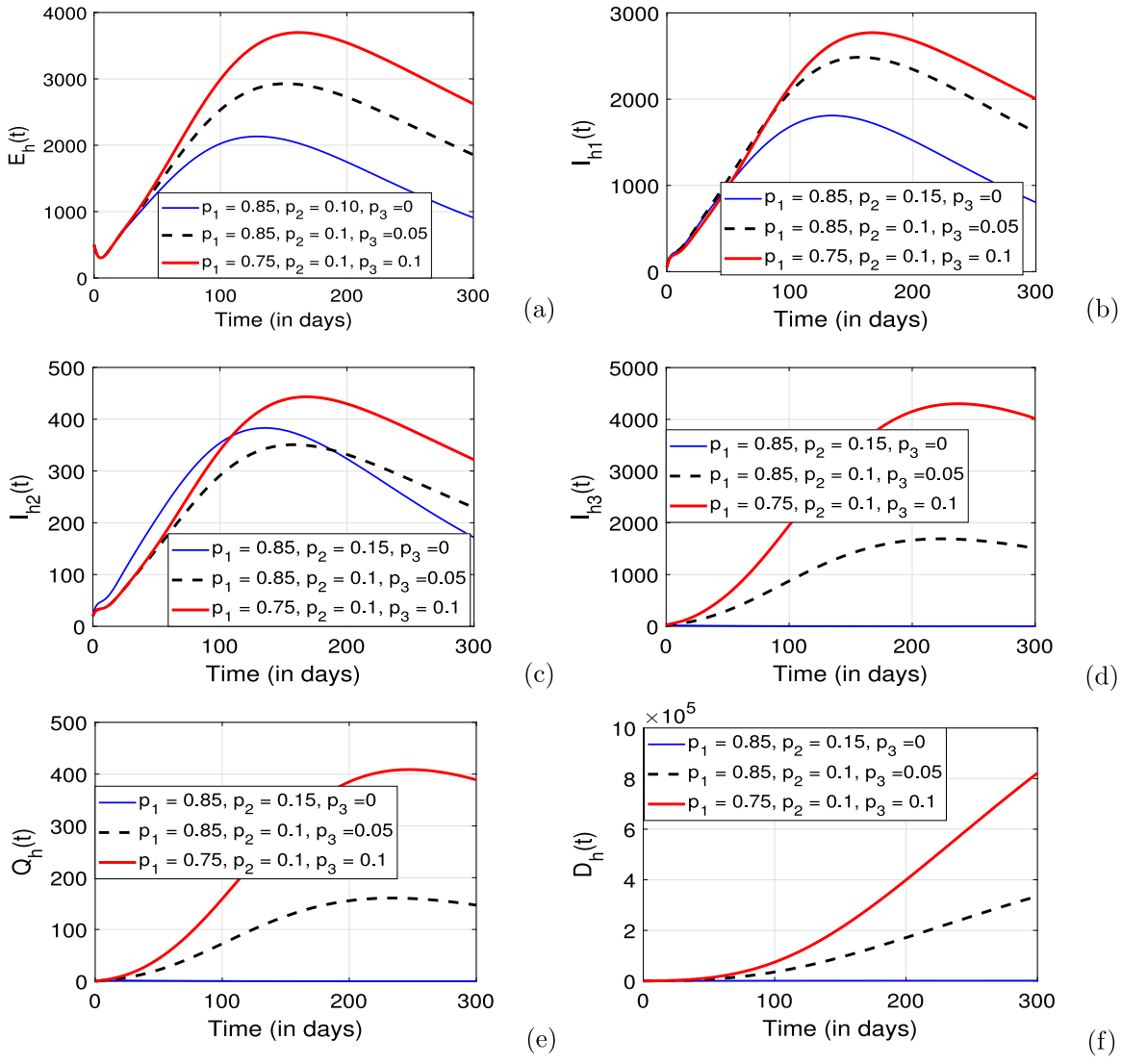

Fig. 6. Variation in epidemic dynamics by fraction of severely infected individuals.

Table 3
Forward-backward sweep iterative method.

Algorithm
1. Subdivide the time interval $[t_0, t_f]$ into N equal subintervals. Set the state variable at different times as $x = x(t)$ and assume a piecewise-constant control $u^{(0)}(t)$, $t \in [t_k, t_{k+1}]$, where $k = 0, 1, 2, \ldots, N-1$.
2. Apply the assumed control $u_j^{(0)}(t)$ to integrate the state system with an initial condition $x(t_0) = \mathbf{x}(0)$, forward in time $[t_0, t_f]$ using the fourth-order Runge–Kutta method, where $\mathbf{x}_0 = (S_h(0), E_h(0), I_{h1}(0), I_{h2}(0), I_{h3}(0), Q_h(0), R_h(0), S_v(0), E_h(0), I_v(0))$.
3. Apply the assumed control $u^{(0)}(t)$ to integrate the costate system with the transversality condition $\vec{\lambda}(t_f) = \lambda_i(t_f)$, $i = 1, 2, 3, \ldots, 10$, backward in time $[t_0, t_f]$ using the fourth-order Runge–Kutta method.
4. Update the control by entering the new state and costate solutions $\vec{x}(t)$ and $\vec{\lambda}(t_f)$, respectively, through the characterization equation (C.2).
5. STOP the algorithm if $\frac{\|\vec{x}^{i+1} - \vec{x}^i\|}{\|\vec{x}^{i+1}\|} < \xi$; otherwise update the control using a convex combination of the current and previous control and GO to step 2. Here, $\vec{x}^i$ is the i^{th} iterative solution of the state system and ξ is an arbitrarily small positive quantity (Tolerance level).

In both scenarios, the disease is eliminated in both the host and the vector when time-dependent preventive control strategies are combined with hospitalization. However, the cost of implementing these strategies affects the timeline for disease extinction. For example, in Fig. 8, when costs are set at $A = 10^{-3}$, disease elimination in both the host and vector occurs after approximately 400 days of intervention. In this case, maximum intensity control efforts cannot be fully implemented. In contrast, when $A = 10^{-5}$ (lower costs), control efforts can be applied at maximum intensity throughout the entire period. This leads to the elimination of the disease in about 100 days for both the host and the vector. Overall, this analysis highlights that while more robust control strategies increase effectiveness in fighting the disease, the costs associated with these strategies significantly affect the timeline for disease extinction.

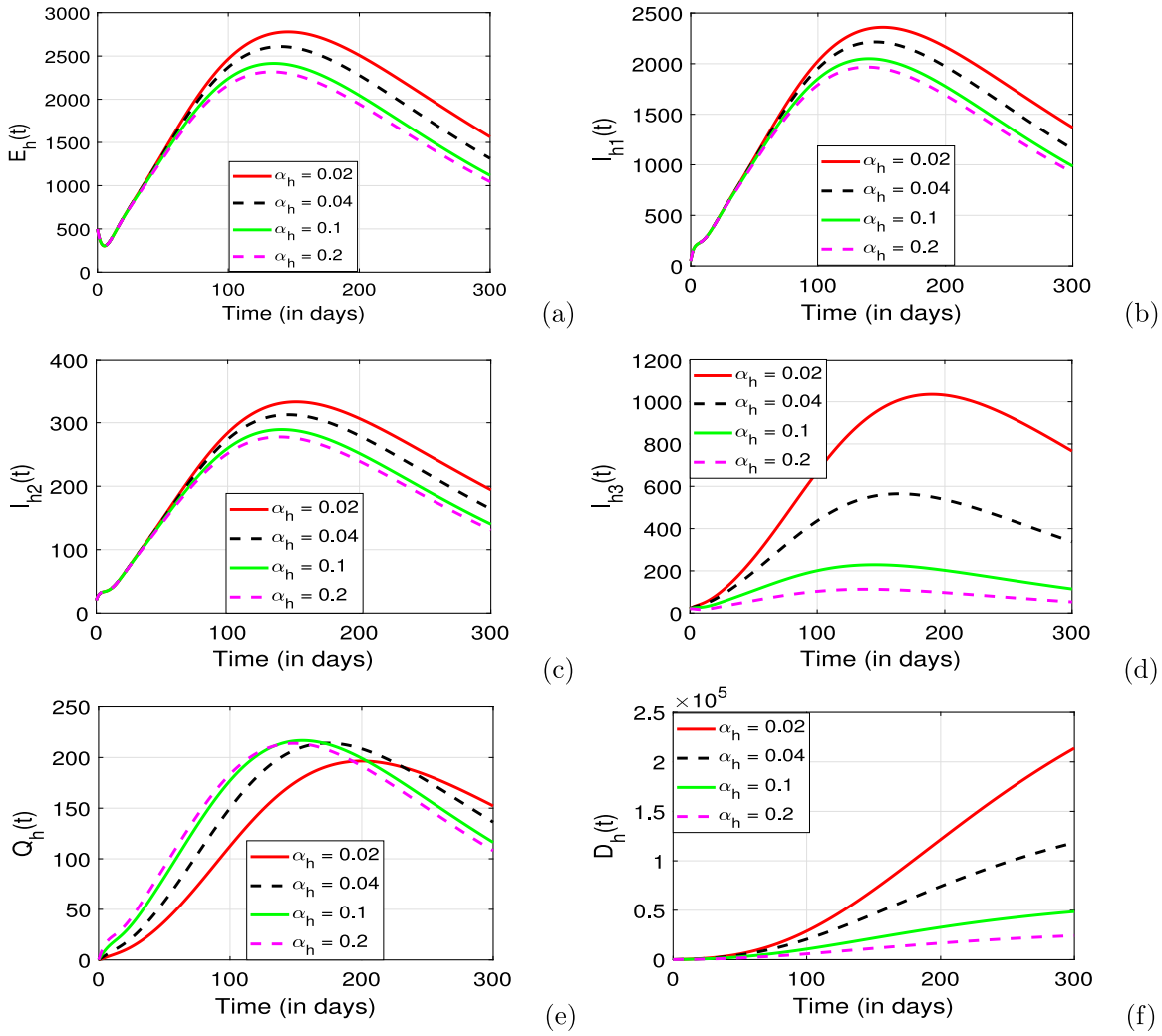

Fig. 7. Variation in epidemic dynamics by treatment rate under unlimited medical resources.

4. Discussion

In this work, we proposed and analyzed a comprehensive mathematical model of dengue fever (DF) that accounts for heterogeneous clinical manifestations, limited medical resources, and time-dependent preventive efforts. The motivation for this study stems from the recognition that the clinical spectrum of dengue ranges widely, from unapparent or asymptomatic infections to severe and fatal cases [5]. Additionally, recent reports indicate an increase in the frequency and severity of dengue outbreaks, emphasizing the urgent need for effective modeling and control strategies. Initially, we examined a basic framework devoid of preventive control measures and resource limitations. In this context, we computed the basic reproduction number, $\mathcal{R}_0$, and investigated how it depends on key model parameters. Our analysis revealed that increases in the mosquito recruitment rate, the proportion of severely infected individuals, and the host-to-vector infection rate significantly elevate $\mathcal{R}_0$, thereby enhancing disease transmission potential. Conversely, an increase in the host's natural mortality rate was found to reduce $\mathcal{R}_0$; however, this is not a practical control measure. These insights underscore the importance of targeted interventions aimed at specific transmission pathways.

Subsequently, we explored the model's dynamic behavior without implementing control efforts. Notably, our analysis demonstrated the presence of a backward bifurcation within the system. This phenomenon is critical for disease control, as it indicates that achieving a reproduction number less than one is not sufficient to guarantee disease eradication. Instead, a stable endemic equilibrium can coexist with the disease-free state, complicating elimination strategies. Our findings align with earlier studies, such as that of Abdelrazec et al. [13], which also identified backward bifurcation phenomena in similar models. Motivated by this complexity, we extended the model to incorporate time-dependent preventive efforts and non-time-dependent hospitalization for severely infected individuals. We formulated an optimal control problem to identify strategies that effectively minimize disease burden and associated costs. To realistically capture healthcare limitations, we employed a nonlinear hospitalization function that reflects the finite capacity of medical facilities. Specifically, as the number of severely infected individuals increases, the rate of hospital admissions saturates, modeling resource constraints accurately. Furthermore, increased healthcare resources correspond to higher hospitalization rates, emphasizing the importance of resource allocation.

Numerical simulations of the extended model revealed that the cost associated with implementing control measures significantly influences the timeline for disease elimination. For instance, with a cost parameter set at 10^{-3}, the disease could be eradicated in approximately 400 days starting from an initial infected population of 1400 and a hospital capacity of 20 beds. In contrast, reducing the cost parameter to 10^{-5} enables sustained

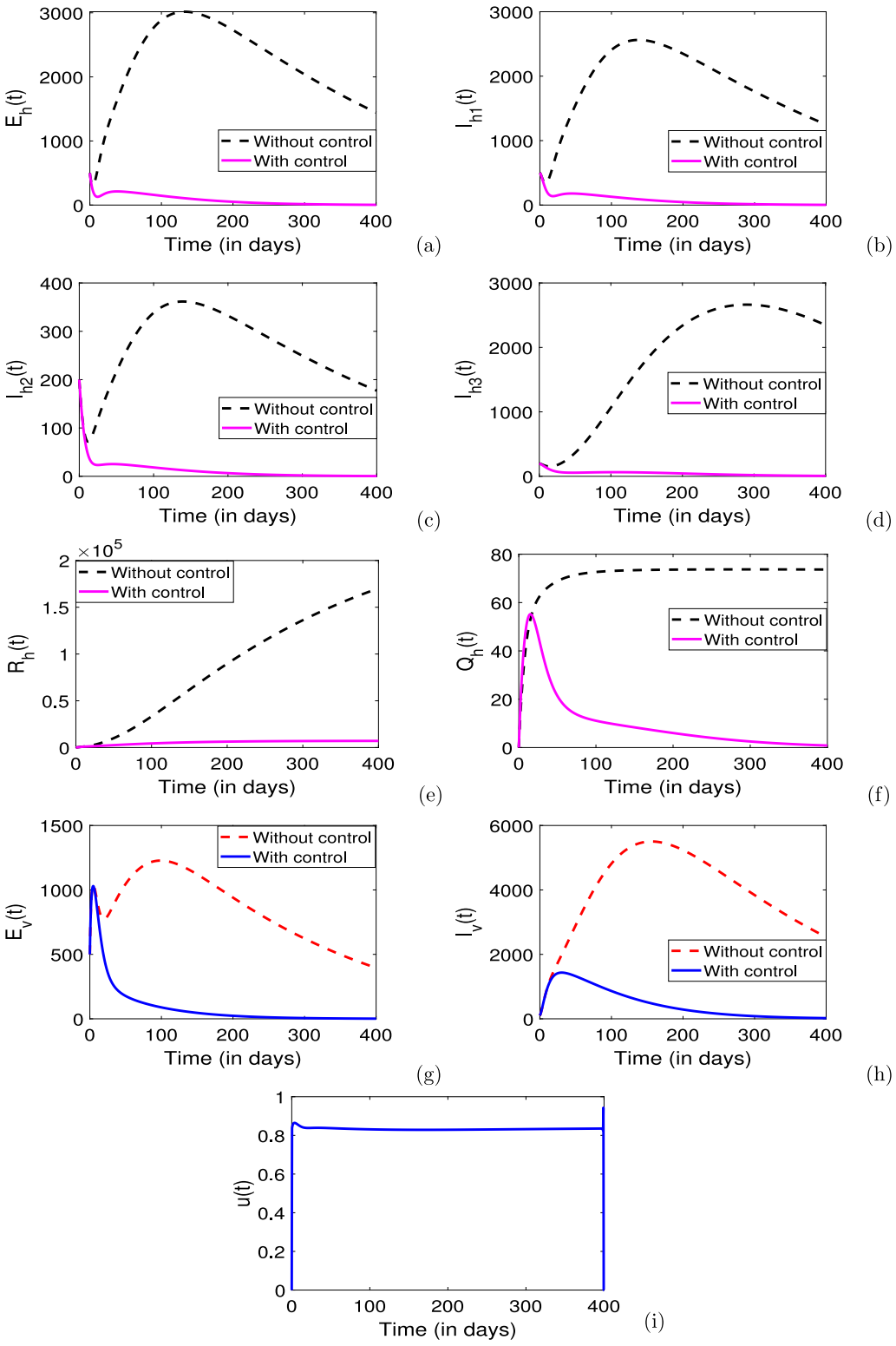

Fig. 8. Variation in epidemic dynamics by time-dependent preventive control strategies, with $A = 10^{-3}$.

efforts, leading to disease elimination in around 100 days under identical initial conditions. These results are consistent with prior studies [31,32], which demonstrated that optimizing preventive strategies not only reduces the disease burden but also alleviates hospital resource utilization.

Overall, this work advances existing dengue modeling frameworks by integrating critical factors such as heterogeneous clinical outcomes, resource limitations, and time-dependent control efforts. Our findings provide valuable insights for policymakers and health authorities, especially in resource-constrained settings, by illustrating how targeted interventions and resource management can accelerate disease control. Nonetheless, the study has certain limitations. Future research could incorporate multiple dengue strains and their interactions, as well as co-infections with other

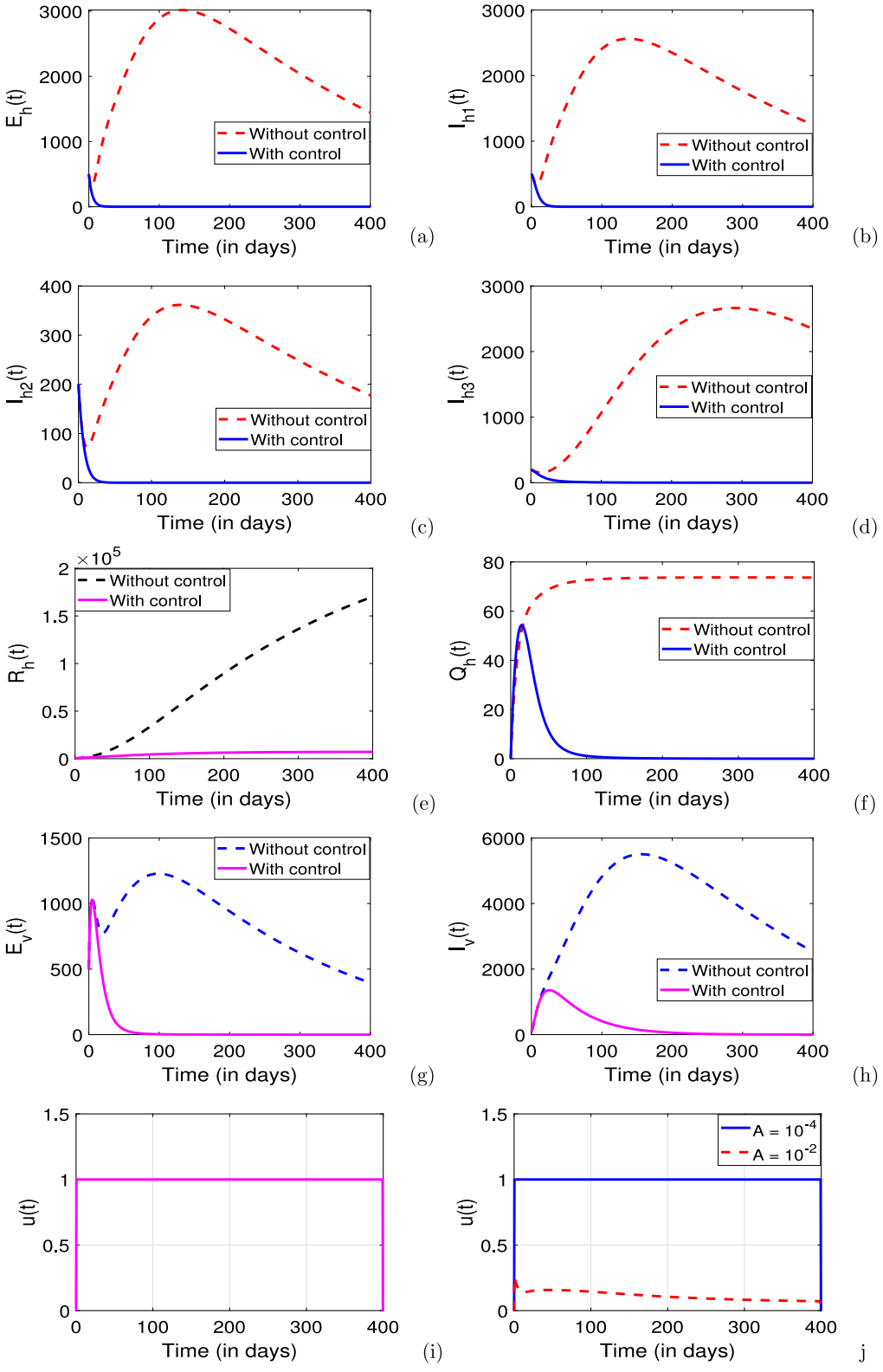

Fig. 9. (a)–(h) Variation in epidemic dynamics by time-dependent preventive control strategies, with $A = 10^{-5}$, (j) Control profile of $u(t)$ with varying costs (A).

arboviruses such as Zika and chikungunya, to better capture the complexity of real-world scenarios. Additionally, integrating climatic variables — such as temperature, rainfall, and humidity — would enhance the model's predictive capacity, given their significant influence on vector development, survival, and disease transmission dynamics.

In conclusion, our study underscores the importance of strategic, resource-aware interventions in controlling dengue fever. By providing a framework that accounts for heterogeneous clinical presentations, limited healthcare capacity, and dynamic control efforts, we contribute valuable tools for designing effective public health responses. Future enhancements along the suggested directions will further refine these models, ultimately supporting more robust and context-specific disease management strategies.

CRediT authorship contribution statement

Salamida Daudi: Writing – original draft, Methodology, Formal analysis, Conceptualization. **Eva Lusekelo:** Writing – original draft, Investigation, Formal analysis. **Mlyashimbi Helikumi:** Writing – original draft, Methodology, Conceptualization. **Steady Mushayabasa:** Writing – review & editing, Supervision, Conceptualization.

Declaration of Generative AI and AI-assisted technologies in the writing process

During the preparation of this work the authors utilized AI to improve language and readability. After using this tool, the authors reviewed and edited the content as needed and take full responsibility for the content of the publication.

Declaration of competing interest

The authors declare that they have no conflicts of interest.

Acknowledgments

Authors are grateful to three anonymous reviewers for their invaluable comments and suggestions, which greatly improved the presentation of this paper. The views, opinions, assumptions or any other information expressed in this article are solely those of the authors. Additionally, all the authors are grateful to their respective institutions for the support during preparation of the manuscript.

Appendix A. The reproduction number

To better understand the proposed framework, we compute the basic reproduction number which quantifies the new cases generated near the disease-free equilibrium (DFE). Through direct calculations one can observe that in the absence of infection, that is, $E_i = 0$, $I_{ij} = 0$ and $Q_h = R_h = 0$, $i = h, v$, $j = 1, 2, 3$ we have $S_i^0 = \frac{\Lambda_i}{\mu_i}$. Thus, the DFE of model (2.1)–(2.10) has the form $\mathcal{E}^0 = (S_h^0, 0, 0, 0, 0, 0, 0, S_v^0, 0, 0)$. Utilizing the next generation matrix method (NGM) [19], it can be verified that the matrices $\mathcal{F}$ and $\mathcal{V}$, which respectively represent the generation of new infection terms and the remaining transfer terms are respectively given (at the disease-free equilibrium) by

$$\mathcal{F} = \begin{pmatrix} 0 & 0 & 0 & 0 & 0 & 0 & \beta_{vh} \\ 0 & 0 & 0 & 0 & 0 & 0 & 0 \\ 0 & 0 & 0 & 0 & 0 & 0 & 0 \\ 0 & 0 & 0 & 0 & 0 & 0 & 0 \\ 0 & 0 & 0 & 0 & 0 & 0 & 0 \\ 0 & \beta_{hv}\frac{\Lambda_v\mu_h}{\Lambda_h\mu_v} & \beta_{hv}\frac{\Lambda_v\mu_h}{\Lambda_h\mu_v} & \beta_{hv}\frac{\Lambda_v\mu_h}{\Lambda_h\mu_v} & \beta_{hv}\frac{\Lambda_v\mu_h}{\Lambda_h\mu_v} & 0 & 0 \\ 0 & 0 & 0 & 0 & 0 & 0 & 0 \end{pmatrix},$$

$$\mathcal{V} = \begin{pmatrix} \mu_h+\gamma_h & 0 & 0 & 0 & 0 & 0 & 0 \\ -p_1\gamma_h & \mu_h+\sigma_{h1} & 0 & 0 & 0 & 0 & 0 \\ -p_2\gamma_h & 0 & \mu_h+\sigma_{h2} & 0 & 0 & 0 & 0 \\ -p_3\gamma_h & 0 & 0 & \mu_h+\alpha_h & 0 & 0 & 0 \\ 0 & 0 & 0 & -\alpha_h & \mu_h+\sigma_{h3}+d_h & 0 & 0 \\ 0 & 0 & 0 & 0 & 0 & \mu_v+\gamma_v & 0 \\ 0 & 0 & 0 & 0 & 0 & -\gamma_v & \mu_v \end{pmatrix}.$$

Thus, the spectral radius of model (2.1)–(2.10), that is $\rho(\mathcal{F}\mathcal{V}^{-1})$, is

$$\mathcal{R}_0 = \sqrt{\frac{\beta_{hv}\Lambda_v\mu_h}{\Lambda_h\mu_v}\frac{\gamma_h}{m_1}\left(\frac{p_1}{m_2}+\frac{p_2}{m_3}+\frac{p_3}{m_4}+\frac{p_3\alpha_h}{m_4m_5}\right)\frac{\beta_{vh}\gamma_v}{\mu_v m_6}}, \tag{A.1}$$

where

$$m_1 = (\gamma_h+\mu_h), \quad m_2 = (\mu_h+\sigma_{h1}), \quad m_3 = (\mu_h+\sigma_{h2}),$$
$$m_4 = (\mu_h+\alpha_h+\delta_h), \quad m_5 = (\mu_h+\sigma_{h3}+d_h), \quad m_6 = (\mu_v+\gamma_v).$$

Table 4
Number of possible positive real roots of (B.2) for $\mathcal{R}_0 < 1$ and $\mathcal{R}_0 > 1$.

Case	a_0	a_1	a_2	$\mathcal{R}_0$	No. of sign changes	No. of possible positive real roots
1	–	–	+	$\mathcal{R}_0 < 1$	1	1
	–	–	–	$\mathcal{R}_0 > 1$	0	0
2	–	+	+	$\mathcal{R}_0 < 1$	1	1
	–	+	–	$\mathcal{R}_0 > 1$	2	0,2
3	+	+	+	$\mathcal{R}_0 < 1$	0	0
	+	+	–	$\mathcal{R}_0 > 1$	1	1
4	+	–	+	$\mathcal{R}_0 < 1$	2	0,2
	+	–	–	$\mathcal{R}_0 > 1$	1	1

Appendix B. Bifurcation analysis

One can easily verify that the endemic equilibrium (EE) of system (2.1)–(2.10) has the form:

$$\begin{aligned}
S_h^* &= \frac{\Lambda_h}{\lambda_{vh}+\mu_h}, \quad E_h^* = \frac{\lambda_{vh}\Lambda_h}{m_1\left(\lambda_{vh}+\mu_h\right)}, \quad I_{h1}^* = \frac{p_1\gamma_h}{m_2}E_h^*, \quad I_{h2}^* = \frac{p_2\gamma_h}{m_3}E_h^*,\\
I_{h3}^* &= \frac{p_3\gamma_h}{m_4}E_h^*, \quad Q_h^* = \frac{p_3\alpha_h\gamma_h}{m_4m_5}E_h^*, \quad R_h^* = \frac{\gamma_h}{\mu_h}\left(\frac{p_1\sigma_{h1}}{m_2}+\frac{p_2\sigma_{h2}}{m_3}+\frac{p_3\left(f\delta_h+\frac{\alpha_h\sigma_{h3}}{m_5}\right)}{m_4}\right)E_h^*,\\
S_v^* &= \frac{\Lambda_v}{\lambda_{hv}+\mu_v}, \quad E_v^* = \frac{\lambda_{hv}\Lambda_v}{m_6\left(\lambda_{hv}+\mu_v\right)}, \quad I_v^* = \frac{\gamma_v\lambda_{hv}\Lambda_v}{m_6\mu_v\left(\lambda_{hv}+\mu_v\right)},\\
N_h^* &= \frac{\Lambda_h}{\mu_h}-\frac{p_3\gamma_h}{\mu_h m_4}\left(\delta_h+\frac{d_h\alpha_h}{m_5}\right)E_h^*, \quad \lambda_{vh} = -\frac{\beta_{vh}I_v^*}{N_h^*}, \quad \lambda_{hv} = \frac{\beta_{hv}(I_{h1}^*+I_{h2}^*+I_{h3}^*+Q_h^*)}{N_h^*}.
\end{aligned} \tag{B.1}$$

Substituting all the other equilibrium points into $E_h^* = \frac{\lambda_{vh}\Lambda_h}{m_1\left(\lambda_{vh}+\mu_h\right)}$ leads to

$$g(E_h^*) = a_2(E_h^*)^2 + a_1E_h^* + a_0, \tag{B.2}$$

where

$$\begin{aligned}
a_2 =& \frac{\mu_v m_1 m_6 p_3\gamma_h^2\left(d_h\alpha_h+m_5\delta_h\right)\left(m_4m_5p_1\beta_{\mathrm{hv}}\mu_h+m_2p_3\left(\alpha_h d_h\mu_v\left[\frac{\beta_{hv}\mu_h}{d_h\mu_v}-1\right]+m_5\delta_h\mu_v\left[\frac{\beta_{hv}\mu_h}{\delta_h\mu_v}-1\right]\right)\right)}{m_2m_4^2m_5^2\mu_h}\\
&-\frac{\mu_v p_3\gamma_h^2p_2\beta_{hv}m_1m_6\left(d_h\alpha_h+m_5\delta_h\right)}{m_3m_4m_5},\\
a_1 =& m_1\gamma_h\left(\frac{\left(m_2m_4m_5p_2+m_3\left(m_4m_5p_1+m_2p_3\left(m_5+\alpha_h\right)\right)\right)\beta_{hv}\left(\beta_{vh}\gamma_v\Lambda_v+m_6\Lambda_h\mu_v\right)}{m_2m_3m_4m_5}\right)\\
&-\frac{2d_hm_6p_3\alpha_h\Lambda_h\mu_v^2}{m_4m_5\mu_h}-\frac{2m_6p_3\delta_h\Lambda_h\mu_v^2}{\mu_hm_4},\\
a_0 =& \frac{m_1m_6\Lambda_h^2\mu_v^2}{\mu_h}\left(1-\frac{\beta_{hv}\Lambda_v\mu_h}{\Lambda_h\mu_v}\frac{\gamma_h}{m_1}\left[\frac{p_1}{m_2}+\frac{p_2}{m_3}+\frac{p_3}{m_4}+\frac{p_3\alpha_h}{m_4m_5}\right]\frac{\beta_{vh}\gamma_v}{\mu_vm_6}\right)\\
=& \frac{m_1m_6\Lambda_h^2\mu_v^2}{\mu_h}(1-\mathcal{R}_0^2).
\end{aligned}$$

We can observe that the number of possible positive real roots the polynomial (B.2) depends on the signs of a_0, a_1 and a_2. Furthermore, one can observe whenever $\mathcal{R}_0 < 1$ it follows that $a_0 > 0$. Making use of the Descartes rule of signs on the quadratic equation, we list the various possibilities for the roots of (B.2) in Table 4.

Based on this analysis we can conclude that the only possibilities are 1, 2 and 4 this leads to the following results:

Theorem B.1. *The model (2.1)–(2.10) admits:*

(i) No endemic equilibrium if $\mathcal{R}_0 > 1$, and case 1 holds.
(ii) A unique endemic equilibrium if $\mathcal{R}_0 > 1$ and cases 3 and 4 holds.
(iii) More than one endemic equilibrium if $\mathcal{R}_0 > 1$ and cases 2 is satisfied.
(iv) More than one endemic equilibrium if $\mathcal{R}_0 < 1$ and case 4 is satisfied.

To support Theorem B.1 we perform the bifurcation analysis of model (2.1)–(2.10) making use of the center manifold theorem presented in [33]. This technique entails investigating the dynamical behaviors of model (2.1)–(2.10) near $\mathcal{W}^0$ and parameter values around $\mathcal{R}_0 = 1$ being governed by Eq. (B.3):

$$u'(t) = au^2 + bu\mu + \mathcal{O}(u^3), \tag{B.3}$$

where μ is the bifurcation parameter, u is the center manifold of system (2.1)–(2.10) at $\mathcal{R}_0 = 1$. We now redefine transmission coefficients as follows: $\beta_{vh} = \xi\beta_{hv}$ where $\xi(\xi > 0)$ is the modification factor. Thus, in this section, we set our bifurcation parameter as $\mu = \beta_{vh}$. Furthermore, the

expression of a and b will be derived in the following discussion. We focus on the simple zero eigenvalue for $D_x f(x_0, \phi)|_{\mathcal{R}_0=1}$, and the corresponding left and right eigenvectors u and w, such that $uw = 1$. The linearization system (2.1)–(2.10) about the DFE leads to:

$$J = \begin{pmatrix}
-\mu_h & 0 & 0 & 0 & 0 & 0 & 0 & 0 & 0 & -\beta_{\text{vh}} \\
0 & -m_1 & 0 & 0 & 0 & 0 & 0 & 0 & 0 & \beta_{\text{vh}} \\
0 & p_1\gamma_h & -m_2 & 0 & 0 & 0 & 0 & 0 & 0 & 0 \\
0 & p_2\gamma_h & 0 & -m_3 & 0 & 0 & 0 & 0 & 0 & 0 \\
0 & p_3\gamma_h & 0 & 0 & -m_4 & 0 & 0 & 0 & 0 & 0 \\
0 & 0 & 0 & 0 & \alpha_h & -m_5 & 0 & 0 & 0 & 0 \\
0 & 0 & \sigma_{h1} & \sigma_{h2} & f\delta_h & \sigma_{h3} & -\mu_h & 0 & 0 & 0 \\
0 & 0 & -\xi\beta_{vh}\frac{\Lambda_v\mu_h}{\Lambda_h\mu_v} & -\xi\beta_{vh}\frac{\Lambda_v\mu_h}{\Lambda_h\mu_v} & -\xi\beta_{vh}\frac{\Lambda_v\mu_h}{\Lambda_h\mu_v} & -\xi\beta_{vh}\frac{\Lambda_v\mu_h}{\Lambda_h\mu_v} & 0 & -\mu_v & 0 & 0 \\
0 & 0 & \xi\beta_{vh}\frac{\Lambda_v\mu_h}{\Lambda_h\mu_v} & \xi\beta_{vh}\frac{\Lambda_v\mu_h}{\Lambda_h\mu_v} & \xi\beta_{vh}\frac{\Lambda_v\mu_h}{\Lambda_h\mu_v} & \xi\beta_{vh}\frac{\Lambda_v\mu_h}{\Lambda_h\mu_v} & 0 & 0 & -m_7 & 0 \\
0 & 0 & 0 & 0 & 0 & 0 & 0 & 0 & \gamma_v & -\mu_v
\end{pmatrix}.$$

It follows that the right and left-eigenvalues are:

$$w_1 = -\frac{\beta_{vh}}{\mu_h}w_{10}, \quad w_2 = \frac{\beta_{vh}w_{10}}{m_1}, \quad w_3 = \frac{p_1\beta_{vh}\gamma_h}{m_1m_2}w_{10}, \quad w_4 = \frac{p_2\beta_{vh}\gamma_h}{m_1m_3}w_{10}, \quad w_5 = \frac{p_3\beta_{vh}\gamma_h}{m_1m_4}w_{10},$$

$$w_6 = \frac{p_3\alpha_h\beta_{vh}\gamma_h}{m_1m_4m_5}w_{10}, \quad w_7 = \frac{\beta_{\text{vh}}\gamma_h\left(m_2m_4m_5p_2\sigma_{h2} + m_3\left(m_4m_5p_1\sigma_{h1} + m_2p_3\alpha_h\sigma_{h3}\right)\right)}{m_1m_2m_3m_4m_5\mu_h}w_{10},$$

$$w_8 = -\xi\beta_{vh}^2\gamma_h\left(\frac{\Lambda_v\mu_h}{\Lambda_h\mu_v}\right)\frac{\left(m_2m_4m_5p_2 + m_3\left(m_4m_5p_1 + m_2p_3\left(m_5+\alpha_h\right)\right)\right)}{m_1m_2m_3m_4m_5\mu_v}w_{10},$$

$$w_9 = \xi\beta_{vh}^2\gamma_h\left(\frac{\Lambda_v\mu_h}{\Lambda_h\mu_v}\right)\frac{\left(m_2m_4m_5p_2 + m_3\left(m_4m_5p_1 + m_2p_3\left(m_5+\alpha_h\right)\right)\right)}{m_1m_2m_3m_4m_5m_6}w_{10}, \quad w_{10} > 0,$$

and

$$u_1 = 0, \quad u_2 = \left(\xi\beta_{vh}\frac{\Lambda_v\mu_h}{\Lambda_h\mu_v}\right)\frac{\left(m_2m_4m_5p_2 + m_3\left(m_4m_5p_1 + m_2p_3\left(m_5+\alpha_h\right)\right)\right)\gamma_h\gamma_v}{m_1m_2m_3m_4m_5m_6}u_{10},$$

$$u_3 = \left(\xi\beta_{vh}\frac{\Lambda_v\mu_h}{\Lambda_h\mu_v}\right)\frac{\gamma_v}{m_2m_6}u_{10}, \quad u_4 = \left(\xi\beta_{vh}\frac{\Lambda_v\mu_h}{\Lambda_h\mu_v}\right)\frac{\gamma_v}{m_3m_6}u_{10}, \quad u_5 = \left(\xi\beta_{vh}\frac{\Lambda_v\mu_h}{\Lambda_h\mu_v}\right)\frac{u_{10}\left(m_5+\alpha_h\right)\gamma_v}{m_4m_5m_6},$$

$$u_6 = \left(\xi\beta_{vh}\frac{\Lambda_v\mu_h}{\Lambda_h\mu_v}\right)\frac{\gamma_v}{m_5m_6}u_{10}, \quad u_7 = 0, \quad u_8 = 0, \quad u_9 = \frac{\gamma_v}{m_6}u_{10}, \quad u_{10} > 0.$$

Let $f_1 = S_h'$, $f_2 = E_h'$, $f_3 = I_{h1}'$, $f_4 = I_{h2}'$, $f_5 = I_{h3}'$, $f_6 = Q_h'$, $f_7 = R_h'$, $f_8 = S_v$, $f_9 = E_v$ and $f_{10} = I_v$, and $x_1 = S_h$, $E_h = x_2$, $I_{h1} = x_3$, $I_{h2} = x_4$, $x_5 = I_{h3}$, $x_6 = Q_h$, $x_7 = R_h$, $x_8 = S_v$, $x_9 = E_v$ and $x_{10} = I_v$. It follows that the second-order partial derivatives (the non-zero elements) are:

$$\frac{\partial^2 f_2}{\partial x_2\partial x_{10}} = \frac{\partial^2 f_2}{\partial x_3\partial x_{10}} = \frac{\partial^2 f_2}{\partial x_4\partial x_{10}} = \frac{\partial^2 f_2}{\partial x_5\partial x_{10}} = \frac{\partial^2 f_2}{\partial x_6\partial x_{10}} = \frac{\partial^2 f_2}{\partial x_7\partial x_{10}} = -\frac{2\beta_{vh}\mu_h}{\Lambda_h},$$

$$\frac{\partial^2 f_9}{\partial x_1\partial x_3} = \frac{\partial^2 f_9}{\partial x_1\partial x_4} = \frac{\partial^2 f_9}{\partial x_1\partial x_5} = \frac{\partial^2 f_9}{\partial x_1\partial x_6} = \frac{\partial^2 f_9}{\partial x_2\partial x_3} = \frac{\partial^2 f_9}{\partial x_2\partial x_4} = \frac{\partial^2 f_9}{\partial x_2\partial x_5} = -\frac{2\xi\beta_{vh}\mu_h^2\Lambda_v}{\Lambda_h^2\mu_v},$$

$$\frac{\partial^2 f_9}{\partial x_2\partial x_6} = \frac{\partial^2 f_9}{\partial x_3\partial x_3} = \frac{\partial^2 f_9}{\partial x_3\partial x_4} = \frac{\partial^2 f_9}{\partial x_3\partial x_5} = \frac{\partial^2 f_9}{\partial x_3\partial x_6} = \frac{\partial^2 f_9}{\partial x_4\partial x_4} = \frac{\partial^2 f_9}{\partial x_4\partial x_5} = -\frac{2\xi\beta_{vh}\mu_h^2\Lambda_v}{\Lambda_h^2\mu_v},$$

$$\frac{\partial^2 f_9}{\partial x_4\partial x_6} = \frac{\partial^2 f_9}{\partial x_4\partial x_7} = \frac{\partial^2 f_9}{\partial x_5\partial x_5} = \frac{\partial^2 f_9}{\partial x_5\partial x_6} = \frac{\partial^2 f_9}{\partial x_5\partial x_7} = \frac{\partial^2 f_9}{\partial x_6\partial x_6} = \frac{\partial^2 f_9}{\partial x_6\partial x_7} = -\frac{2\xi\beta_{vh}\mu_h^2\Lambda_v}{\Lambda_h^2\mu_v},$$

$$\frac{\partial^2 f_9}{\partial x_3\partial x_8} = -\frac{2\beta_{vh}\mu_h}{\Lambda_h}\frac{\partial^2 f_9}{\partial x_4\partial x_8} = \frac{\partial^2 f_9}{\partial x_5\partial x_8} = \frac{\partial^2 f_9}{\partial x_6\partial x_8} = \frac{2\xi\beta_{vh}\mu_h}{\Lambda_h}, \quad \frac{\partial^2 f_2}{\partial x_9\partial\beta_{vh}} = 1,$$

$$\frac{\partial^2 f_8}{\partial x_3\partial\beta_{vh}} = \frac{\partial^2 f_8}{\partial x_4\partial\beta_{vh}} = \frac{\partial^2 f_8}{\partial x_5\partial\beta_{vh}} = \frac{\partial^2 f_8}{\partial x_6\partial\beta_{vh}} = \frac{\xi\mu_h\Lambda_v}{\Lambda_h\mu_v}.$$

Utilizing formulas and results in [33], we compute a and b as presented as follows:

$$
\begin{aligned}
a = & \sum_{i,jk=1}^{5} u_i w_j w_k \frac{\partial^2 f_i(x_0,\phi)}{\partial x_j \partial x_k}|_{\mathcal{R}_0=1} \\
= & \frac{2\xi\beta_{vh}^2\Lambda_v}{\Lambda_h^2\mu_v}\left(1-\frac{\mu_h}{m_1}-\frac{p_1\gamma_h\mu_h}{m_1m_2}\right)\left(\frac{p_1\beta_{vh}\gamma_h}{m_1m_2}+\frac{p_2\beta_{vh}\gamma_h}{m_1m_3}+\frac{p_3\beta_{vh}\gamma_h}{m_1m_4}+\frac{p_3\alpha_h\beta_{vh}\gamma_h}{m_1m_4m_5}\right)w_{10}^2u_9 \\
& + \frac{2\xi\beta_{vh}\mu_h\Lambda_v}{\Lambda_h}\left(\frac{p_1\beta_{vh}\gamma_h}{m_1m_2}+\frac{p_2\beta_{vh}\gamma_h}{m_1m_3}+\frac{p_3\beta_{vh}\gamma_h}{m_1m_4}+\frac{p_3\alpha_h\beta_{vh}\gamma_h}{m_1m_4m_5}\right)w_8w_{10}u_9 \\
& - \frac{2\beta_{vh}\mu_h}{\Lambda_h}\left(\frac{\beta_{vh}}{m_1}+\frac{p_1\beta_{vh}\gamma_h}{m_1m_2}+\frac{p_2\beta_{vh}\gamma_h}{m_1m_3}+\frac{p_3\beta_{vh}\gamma_h}{m_1m_4}+\frac{p_3\alpha_h\beta_{vh}\gamma_h}{m_1m_4m_5}\right)w_{10}^2u_2 \\
& - \frac{2\beta_{vh}\mu_h}{\Lambda_h}\frac{\beta_{vh}\gamma_h\left(m_2m_4m_5p_2\sigma_{h2}+m_3\left(m_4m_5p_1\sigma_{h1}+m_2p_3\alpha_h\sigma_{h3}\right)\right)}{m_1m_2m_3m_4m_5\mu_h}w_{10}^2u_2 \\
& - \frac{2\xi\beta_{vh}\mu_h^2\Lambda_v}{\Lambda_h^2\mu_v}\frac{p_3\alpha_h\beta_{vh}\gamma_h}{m_1m_4m_5}\left(\frac{p_2\beta_{vh}\gamma_h}{m_1m_3}+\frac{p_3\beta_{vh}\gamma_h}{m_1m_4}+\frac{p_3\alpha_h\beta_{vh}\gamma_h}{m_1m_4m_5}\right)w_{10}^2u_9 \\
& - \frac{2\xi\beta_{vh}^2\mu_h^2\Lambda_v}{\Lambda_h^2\mu_v}\frac{\gamma_h\left(m_2m_4m_5p_2\sigma_{h2}+m_3\left(m_4m_5p_1\sigma_{h1}+m_2p_3\alpha_h\sigma_{h3}\right)\right)}{m_1m_2m_3m_4m_5\mu_h} \\
& \times\left(\frac{p_2\beta_{vh}\gamma_h}{m_1m_3}+\frac{p_3\beta_{vh}\gamma_h}{m_1m_4}+\frac{p_3\alpha_h\beta_{vh}\gamma_h}{m_1m_4m_5}\right)w_{10}^2u_9 \\
& - \frac{2\xi\beta_{vh}\mu_h^2\Lambda_v}{\Lambda_h^2\mu_v}\frac{p_3\beta_{vh}\gamma_h}{m_1m_4}\left(\frac{p_2\beta_{vh}\gamma_h}{m_1m_3}+\frac{p_3\beta_{vh}\gamma_h}{m_1m_4}\right)w_{10}^2u_9-\frac{2\xi\beta_{vh}\mu_h^2\Lambda_v}{\Lambda_h^2\mu_v}\left(\frac{p_2\beta_{vh}\gamma_h}{m_1m_3}\right)^2w_{10}^2u_9
\end{aligned}
$$

$$
\begin{aligned}
b = & \sum_{i,jk=1}^{5} u_i w_j \frac{\partial^2 f_i(x_0,\phi)}{\partial x_j \partial\theta}|_{\mathcal{R}_0=1} \\
= & \beta_{vh}\xi\left(\frac{\Lambda_v\mu_h}{\Lambda_h\mu_v}\right)\left(\frac{p_1}{m_2}+\frac{p_2}{m_3}+\frac{p_3(\alpha_h+m_5)}{m_4m_5}\right)\frac{\gamma_h\gamma_v}{m_1m_6}w_{10}u_{10} \\
& + \beta_{vh}^2\gamma_h^2\gamma_v\xi^2\left(\frac{\Lambda_v\mu_h}{\Lambda_h\mu_v}\right)^2\left(\frac{\left(m_2m_4m_5p_2+m_3\left(m_4m_5p_1+m_2p_3\left(m_5+\alpha_h\right)\right)\right)}{m_1m_2m_3m_4m_5m_6}\right)w_{10}u_{10}.
\end{aligned}
$$

Since the coefficient b is positive, system (2.1)–(2.10) undergoes a backward bifurcation at $\mathcal{R}_0 = 1$, if $a > 0$,. Based on this result, we have the following theorem:

Theorem B.2. *At $\mathcal{R}_0 = 1$, model (2.1)–(2.10) admits a backward bifurcation.*

Appendix C. Necessary conditions for the optimality

The optimal control problem (2.18)–(2.27) can be reduced to minimizing the corresponding Hamiltonian with respect to $u(t)$

$$
\mathcal{H}(t,\mathbf{x},\mathbf{u},\lambda) = I_{h1}(t)+I_{h2}(t)+I_{h3}(t)+Q_h(t)+\frac{A}{2}u(t)^2+\lambda_k g_k, \tag{C.1}
$$

where $\lambda = [\lambda_1(t),\lambda_2(t),\ldots,\lambda_{10}(t)]$ are the adjoint variable for a 7 dimensional state, that is., $\mathbf{x} = (S_h, E_h, I_{h1}, I_{h2}, I_{h3}, Q_h, R_h, S_v, E_v, I_v)$, $\mathbf{u} = u(t)$, and g_k is the right hand side of model (2.18)–(2.27) with $k = 1,2,\ldots,10$. The Hamiltonian is constructed to satisfy the first the following relation $\frac{\partial\mathcal{H}}{\partial\mathbf{x}} = -\frac{d\lambda}{dt}$, that is:

$$
\begin{aligned}
\frac{d\lambda_1}{dt} = -\frac{\partial\mathcal{H}}{\partial S_h}, \frac{d\lambda_2}{dt} &= -\frac{\partial\mathcal{H}}{\partial E_h}, \frac{d\lambda_3}{dt} = -\frac{\partial\mathcal{H}}{\partial I_{h1}}, \frac{d\lambda_4}{dt} = -\frac{\partial\mathcal{H}}{\partial I_{h2}}, \frac{d\lambda_5}{dt} = -\frac{\partial\mathcal{H}}{\partial I_{h3}}, \\
\frac{d\lambda_6}{dt} &= -\frac{\partial\mathcal{H}}{\partial Q_h}, \frac{d\lambda_7}{dt} = -\frac{\partial\mathcal{H}}{\partial R_h}, \frac{d\lambda_8}{dt} = -\frac{\partial\mathcal{H}}{\partial S_v}, \frac{d\lambda_9}{dt} = -\frac{\partial\mathcal{H}}{\partial E_v}, \frac{d\lambda_10}{dt} = -\frac{\partial\mathcal{H}}{\partial I_v},
\end{aligned}
$$

such that :

$$
\begin{aligned}
\frac{d\lambda_1}{dt} = & \mu_h\lambda_1+\frac{\beta_{vh}(1-u(t))I_v}{N_h}(\lambda_1-\lambda_2)+\frac{\beta_{hv}(1-u(t))S_v(I_{h1}+I_{h2}+I_{h3}+Q_h)}{N_h^2}(\lambda_9-\lambda_8) \\
& + \frac{\beta_{vh}(1-u(t))I_vS_h}{N_h^2}(\lambda_2-\lambda_1), \\
\frac{d\lambda_2}{dt} = & \mu_h\lambda_2+\gamma_h(\lambda_2-p_1\lambda_3-p_2\lambda_4-p_3\lambda_5)+\frac{\beta_{hv}(1-u(t))S_v(I_{h1}+I_{h2}+I_{h3}+Q_h)}{N_h^2}(\lambda_9-\lambda_8) \\
& + \frac{\beta_{vh}(1-u(t))I_vS_h}{N_h^2}(\lambda_2-\lambda_1), \\
\frac{d\lambda_3}{dt} = & \mu_h\lambda_3+\sigma_{h1}(\lambda_3-\lambda_7)++\frac{\beta_{vh}(1-u(t))I_vS_h}{N_h^2}(\lambda_2-\lambda_1)+\frac{\beta_{hv}(1-u(t))S_v}{N_h}(\lambda_8-\lambda_9), \\
& + \frac{\beta_{hv}(1-u(t))S_v(I_{h1}+I_{h2}+I_{h3}+Q_h)}{N_h^2}(\lambda_9-\lambda_8),
\end{aligned}
$$

$$\frac{d\lambda_4}{dt} = -1 + \mu_h\lambda_4 + \sigma_{h2}(\lambda_4 - \lambda_7) + \frac{\beta_{vh}(1-u(t))I_v S_h}{N_h^2}(\lambda_2 - \lambda_1) + \frac{\beta_{hv}(1-u(t))S_v}{N_h}(\lambda_8 - \lambda_9) + \frac{\beta_{hv}(1-u_1)S_v(I_{h1}+I_{h2}+I_{h3}+Q_h)}{N_h^2}(\lambda_9 - \lambda_8),$$

$$\frac{d\lambda_5}{dt} = -1 + \mu_h\lambda_5 + \delta_h(\lambda_5 - f\lambda_7) + \frac{K_h(\alpha_{h1}-\alpha_{h0})(\lambda_5-\lambda_6)}{K_h + I_{h3}} + \frac{K_h I_{h3}(\alpha_{h1}-\alpha_{h0})(\lambda_6-\lambda_5)}{(K_h+I_{h3})^2} + \frac{\beta_{vh}(1-u(t))I_v S_h}{N_h^2}(\lambda_2-\lambda_1) + \frac{\beta_{hv}(1-u(t))S_v}{N_h}(\lambda_8-\lambda_9) + \frac{\beta_{hv}(1-u(t))S_v(I_{h1}+I_{h2}+I_{h3}+Q_h)}{N_h^2}(\lambda_9-\lambda_8),$$

$$\frac{d\lambda_6}{dt} = -1 + (\mu_h + d_h)\lambda_6 + \sigma_{h3}(\lambda_6 - \lambda_7) + \frac{\beta_{vh}(1-u(t))I_v S_h}{N_h^2}(\lambda_2-\lambda_1) + \frac{\beta_{hv}(1-u(t))S_v}{N_h}(\lambda_8-\lambda_9) + \frac{\beta_{hv}(1-u(t))S_v(I_{h1}+I_{h2}+I_{h3}+Q_h)}{N_h^2}(\lambda_9-\lambda_8),$$

$$\frac{d\lambda_7}{dt} = \mu_h\lambda_7 + \frac{\beta_{vh}(1-u(t))I_v S_h}{N_h^2}(\lambda_2-\lambda_1) + \frac{\beta_{hv}(1-u(t))S_v(I_{h1}+I_{h2}+I_{h3}+Q_h)}{N_h^2}(\lambda_9-\lambda_8),$$

$$\frac{d\lambda_8}{dt} = \mu_v\lambda_8 + \frac{\beta_{hv}(1-u(t))(I_{h1}+I_{h2}+I_{h3}+Q_h)}{N_h^2}(\lambda_8-\lambda_9),$$

$$\frac{d\lambda_9}{dt} = \mu_v\lambda_9 + \gamma_v(\lambda_9 - \lambda_{10}),$$

$$\frac{d\lambda_{10}}{dt} = \mu_v\lambda_{10} + \frac{\beta_{vh}(1-u(t))S_h}{N_h}(\lambda_1 - \lambda_2).$$

with transversality conditions $\lambda_j(t_f) = 0$. Furthermore, by applying the Pontryagin's maximum Principle and the optimality conditions, we have:

$$\frac{\partial \mathcal{H}}{\partial u} = uA_2 - \frac{\beta_{vh}I_v S_h(\lambda_2-\lambda_1)}{N_h} - \frac{\beta_{hv}(I_{h1}+I_{h2}+I_{h3}+Q_h)S_v(\lambda_9-\lambda_8)}{N_h},$$

Thus, optimal controls are characterized by:

$$u^* = \min\left\{u_{\max}, \max\left\{0, \frac{\beta_{vh}I_v S_h(\lambda_2-\lambda_1)}{N_h A_2} + \frac{\beta_{hv}(I_{h1}+I_{h2}+I_{h3}+Q_h)S_v(\lambda_9-\lambda_8)}{N_h A_2}\right\}\right\}, \tag{C.2}$$

where $u_{\max} \leq 1$ represent the feasible upper bounds of the control $u(t)$.

Data availability

No data was used for the research described in the article.

References

[1] Q. Cheng, Q. Jing, R.C. Spear, J.M. Marshall, Z. Yang, P. Gong, Climate and the timing of imported cases as determinants of the dengue outbreak in guangzhou, 2014: Evidence from a mathematical model, PLoS. Negl. Trop. Dis 10 (2) (2016) e0004417, http://dx.doi.org/10.1371/journal.pntd.00044177.

[2] R.Gurgel-Gon, calves, W.K.D. Oliveira, J. Croda, The greatest dengue epidemic in Brazil: surveillance, prevention, and control, Rev. Soc. Bras. Med. Trop 57 (2024) e00203–2024, http://dx.doi.org/10.1590/0037-8682-0113-2024.

[3] F.J. Colón-González, M.O. Sewe, A.M. Tompkins, H. Sjödin, A. Casallas, J. Rocklöv, C. Caminade, R. Lowe, Projecting the risk of mosquito-borne diseases in a warmer and more populated world: A multi-model, multi-scenario intercomparison modelling study, Lancet Planet. Heal. 5 (7) (2021) e404–e414, http://dx.doi.org/10.1016/s2542-5196(21)00132-7.

[4] Q. Zhu, Z. Li, J. Dong, P. Fu, Q. Cheng, J. Cai, H. Gurgel, L. Yang, Spatiotemporal dataset of dengue influencing factors in Brazil based on geospatial big data cloud computing, Sci Data 12 (1) (2025) 712, http://dx.doi.org/10.1038/s41597-025-05045-1.

[5] T.H. Mallhi, A.H. Khan, A. Sarriff, A.S. Adnan, Y.H. Khan, Determinants of mortality and prolonged hospital stay among dengue patients attending tertiary care hospital: a cross-sectional retrospective analysis, BMJ Open 7 (7) (2017) e016805, http://dx.doi.org/10.1136/bmjopen-2017-016805.

[6] A. Sohail, S. Zhong, P.Y. Nguyen, S.L. McGuinness, K. Leder, Dengue fever in immunocompromised patients: A systematic review and meta-analysis, Int. J. Infect. Dis 107 (2024) 272–280, http://dx.doi.org/10.1016/j.ijid.2024.107272.

[7] M.A.M. Khalil, J. Tan, M.A.U. Khalil, S. Awan, M. Rangasami, Predictors of hospital stay and mortality in dengue virus infection—experience from aga khan university hospital Pakistan, in: BMC Res Notes, vol. 7, 2014, p. 504, http://dx.doi.org/10.1186/1756-0500-7-473.

[8] M. Carabali, L.M. Hernandez, M.J. Arauz, L.A. Villar, V. Ridde, Why are people with dengue dying? A scoping review of determinants for dengue mortality, in: BMC Infect Dis, vol. 15, 2015, p. 508, http://dx.doi.org/10.1186/s12879-015-1058-x.

[9] M. Aguiar, V. Anam, K.B. Blyuss, C.D.S. Estadilla, B.V. Guerrero, D. Knopoff, B.W. Kooi, A.K. Srivastav, V. Steindorf, N. Stollenwerk, Mathematical models for dengue fever epidemiology: A 10-year systematic review, Phys. Life Rev 40 (2022) 65–92, http://dx.doi.org/10.1016/j.plrev.2022.07.008.

[10] S.T. Ogunlade, M.T. Meehan, A.I. Adekunle, E.S. McBryde, A systematic review of mathematical models of dengue transmission and vector control: 2010–2020, Viruses 15 (1) (2023) 254, http://dx.doi.org/10.3390/v15010254.

[11] H. Kim, J.E. Kim, S. Lee, C.H. Lee, Potential effects of climate change on dengue transmission dynamics in Korea, PLoS One 13 (6) (2018) e0199205, http://dx.doi.org/10.1371/journal.pone.0199205.

[12] G. Zhu, T. Liu, J. Xiao, B. Zhang, T. Song, Y. Zhang, L. Lin, Z. Peng, A. Deng, W. Ma, Y. Hao, Effects of human mobility, temperature, and mosquito control on the spatiotemporal transmission of dengue, Sci. Total. Env. 651 (2019) 969–978, http://dx.doi.org/10.1016/j.scitotenv.2018.09.182.

[13] A. Abdelrazec, J. Bélair, C. Shan, H. Zhu, Modeling the spread and control of dengue with limited public health resources, Math. Biosci. 271 (2016) 136–145, http://dx.doi.org/10.1016/j.mbs.2015.11.004.

[14] N.I. Hamdan, A. Kilicman, Mathematical modelling of dengue transmission with intervention strategies using fractional derivatives, Bull. Math. Biol. 84 (12) (2022) 138, http://dx.doi.org/10.1007/s11538-022-01096-2.

[15] L. Zou, J. Chen, X. Feng, S. Ruan, Analysis of a dengue model with vertical transmission and application to the 2014 dengue outbreak in Guangdong province, China. Bull Math Biol 80 (2018) 2633–2651, http://dx.doi.org/10.1007/s11538-018-0480-9.
[16] B. Adams, M. Boots, How important is vertical transmission in mosquitoes for the persistence of dengue? Insights from a mathematical model, Epidemics 2 (1) (2010) 1–10, http://dx.doi.org/10.1016/j.epidem.2010.01.001.
[17] M.C. Castro, M.E. Wilson, D.E. Bloom, Disease and economic burdens of dengue, Lancet Infect. Dis. 17 (3) (2017) e70–e78, http://dx.doi.org/10.1016/s1473-3099(16)30545-x.
[18] N.M.S. Sansone, M.N. Boschiero, F.A.L. Marson, Dengue outbreaks in Brazil and latin america: The new and continuing challenges, Int. J. Infect. Dis. 147 (2024) 107192, http://dx.doi.org/10.1016/j.ijid.2024.107192.
[19] P.van.den. Driessche, J. Watmough, Reproduction number and subthreshold endemic equilibria for compartment models of disease transmission, Math. Biosci. 180 (2002) 29–48, http://dx.doi.org/10.1016/s0025-5564(02)00108-6.
[20] M. Chan, M.A. Johansson, The incubation periods of dengue viruses, PLoS One 7 (11) (2012) e50972, http://dx.doi.org/10.1371/journal.pone.0050972.
[21] E. Lusekelo, M. Helikumi, D. Kuznetsov, S. Mushayabasa, Quantifying the potential impact of mass media campaigns on mitigating the spread of chikungunya virus during outbreaks in heterogeneous populations, Informatics Med. Unlocked 40 (2023) 101296, http://dx.doi.org/10.1016/j.imu.2021.100570.
[22] E. Lusekelo, M. Helikumi, D. Kuznetsov, S. Mushayabasa, Quantifying the effects of temperature and predation on the growth of aedes mosquito population, Model. Earth Syst. Env. 9 (3) (2023) 3193–3206, http://dx.doi.org/10.1007/s40808-022-01687-x.
[23] E. Lusekelo, M. Helikumi, D. Kuznetsov, S. Mushayabasa, Dynamic modelling and optimal control analysis of a fractional order chikungunya disease model with temperature effects, Results Control. Optim. 10 (2023) 100206, http://dx.doi.org/10.1016/j.rico.2023.100206.
[24] X. Feng, X. Huo, B. Tang, S. Tang, K. Wang, J. Wu, Modelling and analyzing virus mutation dynamics of chikungunya outbreaks, Sci Rep 9 (1) (2019) 2860, http://dx.doi.org/10.1038/s41598-019-38792-4.
[25] L. Cai, X. Li, N. Tuncer, M. Martcheva, A.A. Lashari, Optimal control of a malaria model with asymptomatic class and superinfection, Math. Biosci. 288 (2017) 94–108, http://dx.doi.org/10.1016/j.mbs.2017.03.003.
[26] E.S. Kevin, J. Abraham, T.C. Prakash, J.A. Merin, A. Ambika, A comprehensive review of the recent advancements in the development of a dengue vaccine: In the hour of need, Int. J Pharm. Biosci 6 (1) (2025) 1–9, http://dx.doi.org/10.22376/ijpbs.v16i2.39.
[27] M.A. Korsah, S.T. Johnston, K.E. Tiedje, K.P. Day, J.A. Flegg, C.R. Walker, Mathematical assessment of the role of intervention programs for malaria control, Bull. Math. Biol. 86 (8) (2024) 91, http://dx.doi.org/10.1007/s11538-024-01321-0.
[28] L. S Pontryagin, Mathematical Theory of Optimal Processes, Routledge, 2018, http://dx.doi.org/10.1201/9780203749319.
[29] S. Marino, I.B. Hogue, C.J. Ray, D.E. Kirschner, A methodology for performing global uncertainty and sensitivity analysis in systems biology, J. Theoret. Biol. 254 (1) (2008) 178–196, http://dx.doi.org/10.1016/j.jtbi.2008.04.011.
[30] S. Lenhart, J.T. Workman, Optimal Control Applied To Biological Models, Chapman and Hall/CRC, 2007, http://dx.doi.org/10.1201/9781420011418.
[31] Shim E., Optimal dengue vaccination strategies of seropositive individuals, Math. Biosci. Eng. 16 (3) (2019) 1171–1189, http://dx.doi.org/10.3934/mbe.2019056.
[32] W. Bock, Y. Jayathunga, Optimal control of a multi-patch dengue model under the influence of wolbachia bacterium, Math. Biosci. Eng. 315 (2019) 108219, http://dx.doi.org/10.1016/j.mbs.2019.108219.
[33] C. Castillo-Chavez, B. Song, Dynamical models of tuberculosis and their applications, Math. Biosci. 1 (2) (2004) 361–404, http://dx.doi.org/10.3934/mbe.2004.1.361.